www.nature.com/neuro /April 2024 Vol. 27 No. 4

nature neuroscience

GluK2 detects cold

nature neuroscience

Article

https://doi.org/10.1038/s41593-024-01585-8

The kainate receptor GluK2 mediates cold sensing in mice

Received: 23 February 2023

Accepted: 23 January 2024

Published online: 11 March 2024

Check for updates

Wei Cai[1,2,7], Wenwen Zhang[1,2,7], Qin Zheng[3,4,7], Chia Chun Hor[5], Tong Pan[1,2], Mahar Fatima[5], Xinzhong Dong[4,6], Bo Duan[5] ✉ & X. Z. Shawn Xu[1,2] ✉

Thermosensors expressed in peripheral somatosensory neurons sense a wide range of environmental temperatures. While thermosensors detecting cool, warm and hot temperatures have all been extensively characterized, little is known about those sensing cold temperatures. Though several candidate cold sensors have been proposed, none has been demonstrated to mediate cold sensing in somatosensory neurons in vivo, leaving a knowledge gap in thermosensation. Here we characterized mice lacking the kainate-type glutamate receptor GluK2, a mammalian homolog of the *Caenorhabditis elegans* cold sensor GLR-3. While GluK2 knockout mice respond normally to heat and mechanical stimuli, they exhibit a specific deficit in sensing cold but not cool temperatures. Further analysis supports a key role for GluK2 in sensing cold temperatures in somatosensory DRG neurons in the periphery. Our results reveal that GluK2—a glutamate-sensing chemoreceptor mediating synaptic transmission in the central nervous system—is co-opted as a cold-sensing thermoreceptor in the periphery.

Temperature has a profound impact on the life of all organisms on Earth[1,2]. To survive and adapt to the ever-changing environment, animals and humans have evolved a specialized somatosensory system to detect temperature changes in the environment, thereby adjusting their behavior and physiology accordingly[1,2]. A central player in this process is molecular thermosensors that act in peripheral somatosensory neurons to sense a wide range of thermal cues, such as cold, cool, warm and hot temperatures[1,2]. Research in the past three decades has identified thermosensors detecting cool, warm and hot temperatures[1]. For example, genetic studies in mice have uncovered a trio of TRP channels (TRPV1, TRPM3 and TRPA1) essential for sensing hot temperatures[3], while TRPM2 is found to be required for detecting warm temperatures[4,5]. Several other TRP channels have also been suggested as thermosensors detecting warm and hot temperatures, such as TRPV2, TRPV3, TRPV4, TRPM4 and TRPM5, though it remains unclear whether they mediate warm and hot sensing in vivo[1]. In addition, the menthol receptor TRPM8 is essential for sensing cool temperatures[6,7]. However, little is known about the thermosensors specialized in detecting cold temperatures[8]. Though several candidates, particularly those thermosensitive TRP channels, have been proposed as cold sensors, their roles in mediating cold sensing in somatosensory neurons in vivo have not been validated[1,8]. As such, the molecular identities of cold sensors remain elusive, leaving a knowledge gap in our understanding of thermosensation.

Ionotropic glutamate receptors (iGluRs), including kainate, AMPA and NMDA receptors, are glutamate-gated cation channels[9]. These chemical-sensing receptors are primarily expressed in the brain where they sense and transmit glutamate signals to mediate synaptic transmission[9]. The kainate receptor GluK2 has emerged as a novel class of candidate cold sensor. This hypothesis is inspired by the observation that GLR-3, a *Caenorhabditis elegans* homolog of GluK2, mediates cold sensing in *C. elegans*[10]. Expression of GluK2 in heterologous systems confers cold sensitivity, indicating that GluK2 can function as a cold sensor in vitro[10]. The activation threshold of GluK2 is ~18 °C (ref. 10),

[1]Life Sciences Institute, University of Michigan, Ann Arbor, MI, USA. [2]Department of Molecular and Integrative Physiology, University of Michigan, Ann Arbor, MI, USA. [3]Department of Anesthesiology and Critical Care Medicine, Johns Hopkins University School of Medicine, Baltimore, MD, USA. [4]The Solomon H. Snyder Department of Neuroscience, Johns Hopkins University School of Medicine, Baltimore, MD, USA. [5]Department of Molecular, Cellular and Developmental Biology, University of Michigan, Ann Arbor, MI, USA. [6]Howard Hughes Medical Institute, Johns Hopkins University School of Medicine, Baltimore, MD, USA. [7]These authors contributed equally: Wei Cai, Wenwen Zhang, Qin Zheng. ✉e-mail: bduan@umich.edu; shawnxu@umich.edu

https://doi.org/10.1038/s41593-024-01585-8

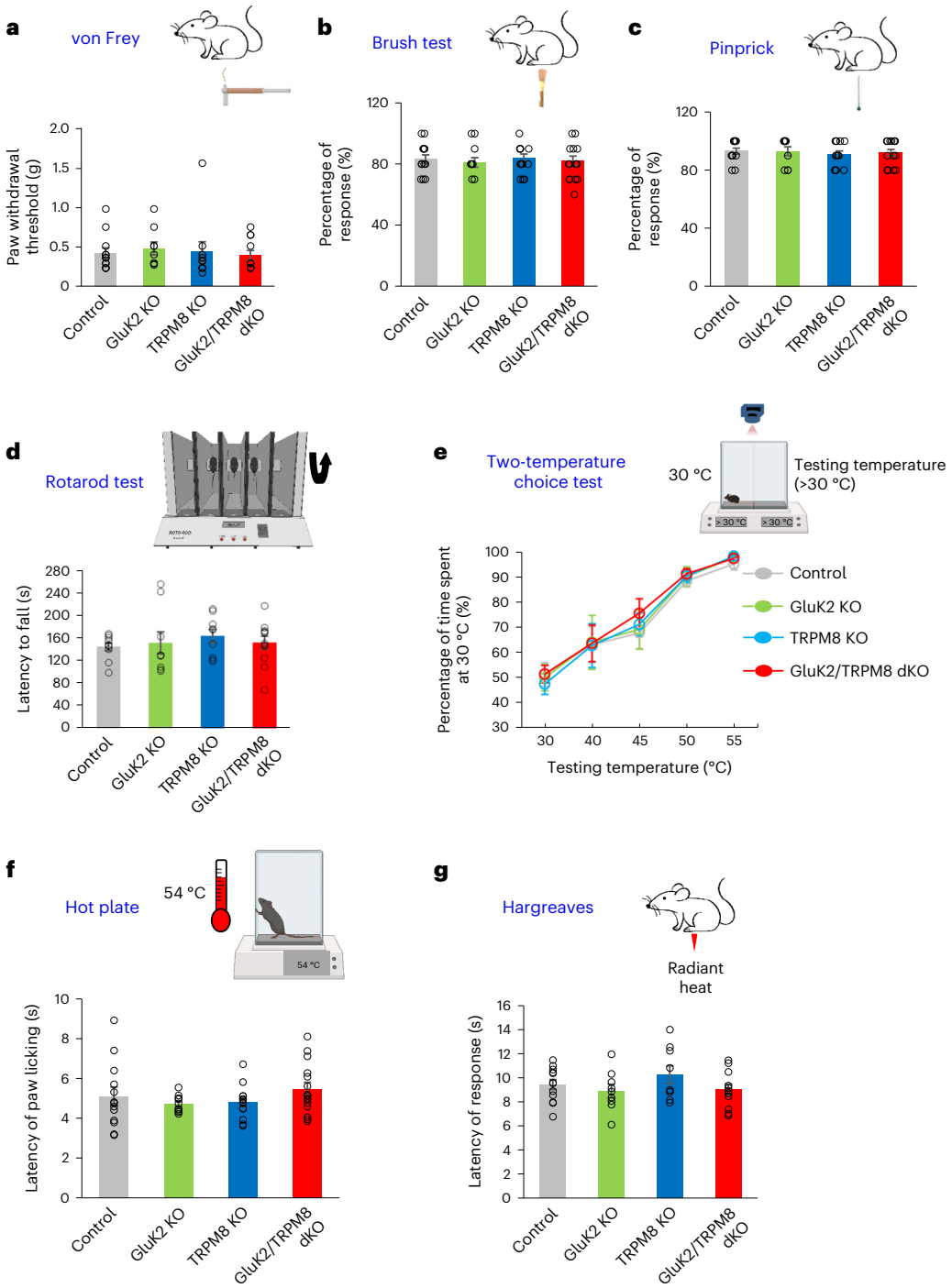

Fig. 1 | GluK2 KO mice respond normally to mechanical and heat stimuli. **a**, GluK2 KO mice behave normally in the von Frey test measuring the mouse's response to punctate mechanical stimuli. Error bars, s.e.m. *P* values: all >0.05 (one-way ANOVA with Tukey's test). Sample size: control $n = 12$, GluK2 KO $n = 9$, TRPM8 KO $n = 10$, GluK2/TRPM8 dKO $n = 11$. **b**, GluK2 KO mice behave normally in the brush test measuring the mouse's response to dynamic mechanical stimuli. Error bars, s.e.m. *P* values: all >0.05 (one-way ANOVA with Tukey's test). Sample size: control $n = 13$, GluK2 KO $n = 10$, TRPM8 KO $n = 13$, GluK2/TRPM8 dKO $n = 15$. **c**, GluK2 KO mice behave normally in the pinprick test measuring the mouse's response to noxious mechanical stimuli. Error bars, s.e.m. *P* values: all >0.05 (one-way ANOVA with Tukey's test). Sample size: control $n = 13$, GluK2 KO $n = 10$, TRPM8 KO $n = 13$, GluK2/TRPM8 dKO $n = 15$. **d**, GluK2 KO mice behave normally in the rotarod test measuring the mouse's locomotion. Error bars, s.e.m. *P* values: all >0.05 (one-way ANOVA with Tukey's test). Sample size: control $n = 10$, GluK2 KO $n = 9$, TRPM8 KO $n = 9$, GluK2/TRPM8 dKO $n = 12$. **e**, GluK2 KO mice respond normally to heat in the two-temperature choice test. Error bars, s.e.m. *P* values: all >0.05 (one-way ANOVA with Tukey's test). Sample size: control $n = 14$, GluK2 KO $n = 9$, TRPM8 KO $n = 12$, GluK2/TRPM8 dKO $n = 10$. **f**, GluK2 KO mice show normal heat nociception in the hot plate assay. The latency of forepaw licking was quantified. Error bars, s.e.m. *P* values: all >0.05 (one-way ANOVA with Tukey's test). Sample size: control $n = 13$, GluK2 KO $n = 10$, TRPM8 KO $n = 13$, GluK2/TRPM8 dKO $n = 15$. **g**, GluK2 KO mice show normal heat nociception in the Hargreaves assay. The latency of paw withdrawal was quantified. Error bars, s.e.m. *P* values: all >0.05 (one-way ANOVA with Tukey's test). Sample size: control $n = 12$, GluK2 KO $n = 9$, TRPM8 KO $n = 9$, GluK2/TRPM8 dKO $n = 11$. Note: all data are presented as mean ± s.e.m. Wild-type and heterozygous littermate mice were used as the controls in all panels. Both male and female mice were tested, and no significant difference between them was observed (Supplementary Fig. 1).

which is substantially lower than that of TRPM8 (~23–28 °C)[11–13]. Surprisingly, GluK2 does not depend on its channel function for cold sensing but instead acts as a novel non-channel type of metabotropic cold sensor in heterologous systems, which transmits cold signals through G protein signaling[10]. This sets GluK2 apart from classical thermosensors such as the aforementioned thermosensitive TRP family channels, all of which are temperature-gated ion channels[1,2,14]. Besides the brain, GluK2 is expressed in dorsal root ganglion (DRG) neurons that directly sense temperature cues in the environment[10]; notably, the expression pattern of GluK2 in the DRG is largely nonoverlapping with those thermosensitive TRP channels[15,16]. Despite these interesting observations, it is not known whether GluK2 mediates cold sensing in DRG neurons in vivo. Nor is it clear whether GluK2 has any physiological roles in cold sensing at the organismal level.

Here, we interrogated the role of GluK2 in somatosensation in mice. We found that while GluK2 knockout (KO) mice respond normally to mechanical and heat stimuli, they exhibit a specific deficit in sensing cold rather than cool temperatures, and are also defective in cold nociception. This reveals a specific role of GluK2 in cold sensing. Selective deletion of GluK2 from DRG neurons led to similar cold-sensing phenotypes, suggesting that GluK2 functions in DRG neurons to mediate cold sensing. Functional recording of DRG neurons both in vitro and in vivo further supports a specific role of GluK2 in sensing cold rather than cool temperatures in these primary somatosensory neurons. Our results identify an unexpected function of GluK2—a kainate receptor best known to transmit chemical synaptic signals in the central nervous system—in sensing cold temperatures in the periphery.

Results

GluK2 KO mice respond normally to mechanical stimuli

Though GluK2 is best known for its function in transmitting synaptic glutamate signals in the brain, it is also expressed in the peripheral nervous system, particularly in DRG somatosensory neurons[10,15,16], raising the possibility that GluK2 may have a role in somatosensation. To test this idea, we characterized somatosensory behaviors of GluK2 KO mice. We first tested how GluK2 KO mice respond to mechanical stimuli using several behavioral assays. We found that compared with control littermates, GluK2 KO mice showed normal responses in the von Frey assay and the brush assay which measure the animal's sensitivity to punctate and dynamic mechanical stimuli[17], respectively (Fig. 1a,b and Supplementary Fig. 1a,b). To test mechanical nociception, we performed the pinprick assay, but observed no defect in GluK2 KO mice (Fig. 1c and Supplementary Fig. 1c). Mice lacking TRPM8, the menthol receptor essential for cool sensing[6,7,12,13], as well as GluK2/TRPM8 double knockout (dKO) mice, also exhibited no notable phenotype in all three mechanosensation assays (Fig. 1a–c and Supplementary Fig. 1a–c). All three types of KO mice showed normal locomotion in the rotarod test (Fig. 1d and Supplementary Fig. 1d). These results indicate that GluK2 is not required for mice to sense mechanical stimuli.

GluK2 KO mice respond normally to heat

We next checked the sensitivity of GluK2 KO mice to heat. We first conducted the two-temperature choice assay which assesses temperature preference and avoidance[6]. In this behavioral assay, animals were allowed to choose between their preferred temperature (30 °C) and a higher testing temperature varying from 30 °C to 55 °C, which covered the range of warm and hot temperatures (Fig. 1e). No defect was detected in GluK2 KO mice in this assay (Fig. 1e and Supplementary Fig. 1e), indicating that GluK2 KO mice possessed normal sensitivity to heat. To test heat nociception, we performed the hot plate assay and the Hargreaves assay, and found that GluK2 KO mice responded normally in both assays (Fig. 1f,g and Supplementary Fig. 1f,g), indicating that heat nociception is preserved in GluK2 KO mice. Similar results were obtained with TRPM8 KO and GluK2/TRPM8 dKO mice in all three heat-sensing tests (Fig. 1e–g and Supplementary Fig. 1e–g). It thus appears that GluK2 is not required for mice to sense heat.

GluK2 KO mice are defective in sensing cold temperatures

To test cold sensitivity, we performed the two-temperature choice assay in which mice were allowed to choose between their preferred temperature (30 °C) and a lower testing temperature varying from 30 °C to 5 °C, covering the range of cool (30–15 °C) and cold (<15 °C) temperatures[6] (Fig. 2a–d). TRPM8 KO mice displayed a severe deficit in avoiding cool temperatures down to 15 °C (Fig. 2b and Supplementary Fig. 2a), supporting the notion that TRPM8 is a cool sensor. Notably, when the testing temperature reached the cold range (<15 °C), no significant difference was observed between TRPM8 KO mice and littermate control mice (Fig. 2b), consistent with previous reports that TRPM8 is not required for sensing cold temperatures[6,7]. By contrast, we observed no defect in GluK2 KO mice at all tested temperatures (Fig. 2b and Supplementary Fig. 2a). The lack of a phenotype in GluK2 KO mice in the cool temperature range is expected, as TRPM8 is the principle cool sensor with a relatively low activation threshold. This suggests that GluK2 does not contribute to cool sensing, which is consistent with its relatively high activation threshold[10].

The absence of a phenotype in GluK2 KO mice within the cold temperature range is not surprising, as TRPM8 is still functional in these mice. Though TRPM8 is classified as a cool sensor owing to its relatively low activation threshold, it retains activity at cold temperatures[12,13], and is thus expected to sense cold temperatures in GluK2 KO mice. We therefore tested GluK2/TRPM8 dKO mice and found that indeed the dKO mice possessed a strong defect at cold temperatures in the two-temperature choice assay when compared with control littermates or TRPM8 KO mice (Fig. 2b), revealing an important role for GluK2 in mediating cold sensing in mice.

To provide additional evidence, we assessed the mouse's sensitivity to cool and cold temperature stimuli by testing paw withdrawal responses evoked by low-temperature water droplets applied to their paw (Fig. 2e–h). Unlike the two-temperature choice assay that tests

Fig. 2 | GluK2 KO mice are defective in cold sensing. a–d, GluK2/TRPM8 dKO and cKO mice are defective in sensing cold temperatures in the two-temperature choice assay. **a**, Schematic. **b**, GluK2/TRMP8 dKO mice are defective in cold sensing. Sample size: control $n = 10$, GluK2 KO $n = 14$, TRPM8 KO $n = 13$, GluK2/TRPM8 dKO $n = 13$. **c**, GluK2 cKO^{Avil}/TRPM8 KO mice are defective in cold sensing. Sample size: control $n = 10$, GluK2 cKO^{Avil} $n = 6$, TRPM8 KO $n = 15$, GluK2 cKO^{Avil}/TRPM8 KO $n = 17$. **d**, GluK2 cKO^{Pirt}/TRPM8 KO mice are defective in cold sensing. Sample size: control $n = 15$, GluK2 cKO^{Pirt} $n = 11$, TRPM8 KO $n = 18$, GluK2 cKO^{Pirt}/TRPM8 KO $n = 21$. $^{*}P < 0.05$, $^{**}P < 0.01$ (one-way ANOVA with Tukey's test, compared with control). $^{\#}P < 0.05$, $^{\#\#}P < 0.01$ (one-way ANOVA with Tukey's test, compared with TRPM8 KO). **e**, TRPM8 KO but not GluK2 KO mice are defective in sensing cool temperature (18 °C water droplet) in the paw withdrawal assay. Error bars, s.e.m. Sample size: control $n = 15$, GluK2 KO $n = 9$, TRPM8 KO $n = 15$, GluK2/TRPM8 dKO $n = 14$. $^{**}P = 6.9 \times 10^{-6}$ (TRPM8 KO versus control), $^{**}P = 1.3 \times 10^{-6}$ (GluK2/TRPM8 dKO versus control), one-way ANOVA with Tukey's test. **f**, GluK2/TRPM8 dKO mice are defective in sensing cold temperature (0 °C water droplet). Sample size: control $n = 15$, GluK2 KO $n = 9$, TRPM8 KO $n = 15$, GluK2/TRPM8 KO $n = 14$. $^{**}P = 1.8 \times 10^{-11}$ (GluK2/TRPM8 dKO versus control), one-way ANOVA with Tukey's test. **g**, TRPM8 KO but not GluK2 cKO^{Pirt} mice are defective in cool sensing. Sample size: control $n = 10$, GluK2 cKO^{Pirt} $n = 11$, TRPM8 KO $n = 15$, GluK2 cKO^{Pirt}/TRPM8 KO $n = 13$. $^{**}P = 5.3 \times 10^{-5}$ (TRPM8 KO versus control), $^{**}P = 4.8 \times 10^{-5}$ (GluK2 cKO^{Pirt}/TRPM8 KO versus control), one-way ANOVA with Tukey's test. **h**, GluK2 cKO^{Pirt}/TRPM8 KO mice are defective in cold sensing. Sample size: control $n = 10$, GluK2 cKO^{Pirt} $n = 11$, TRPM8 KO $n = 15$, GluK2 cKO^{Pirt}/TRPM8 dKO $n = 13$. $^{**}P = 1.4 \times 10^{-6}$ (GluK2 cKO^{Pirt}/TRPM8 KO versus control), one-way ANOVA with Tukey's test. Note: all error bars, s.e.m. All data are presented as mean ± s.e.m. Wild-type and heterozygous littermates were used as the controls in all panels. Both male and female mice were assayed, except in **c** where only males were tested because of a germline-leak concern in Avil-Cre females. No significant difference between males and females was observed (Supplementary Fig. 2).

https://doi.org/10.1038/s41593-024-01585-8

thermal preference and avoidance, this assay offers a more direct assessment of the mouse's avoidance responses to temperature cues. As a control, we found that mice showed minimal or no response to water with temperature close to their paw's skin surface temperature (27 °C) (Extended Data Fig. 1 and Supplementary Table 1). By contrast, mice responded robustly to cool temperature (18 °C) water mostly by lifting their paw (Fig. 2e, Supplementary Fig. 2c and Supplementary Table 1). Mice exhibited a more robust response to cold temperature (0 °C) water by lifting their paw followed by flinching and/or licking (Fig. 2f, Supplementary Fig. 2d and Supplementary Table 1). While TRPM8 KO mice displayed a severe deficit in response to cool temperature stimuli (Fig. 2e, Supplementary Fig. 2c and Supplementary Table 1), GluK2 KO mice responded normally (Fig. 2e, Supplementary Fig. 2c and Supplementary Table 1), further suggesting that GluK2 is not important for mice to sense cool temperatures. Strikingly, while neither GluK2 KO nor TRPM8 KO mice showed a significant defect in response to cold temperatures (Fig. 2f, Supplementary Fig. 2d and Supplementary Table 1), GluK2/TRPM8 dKO mice manifested a strong

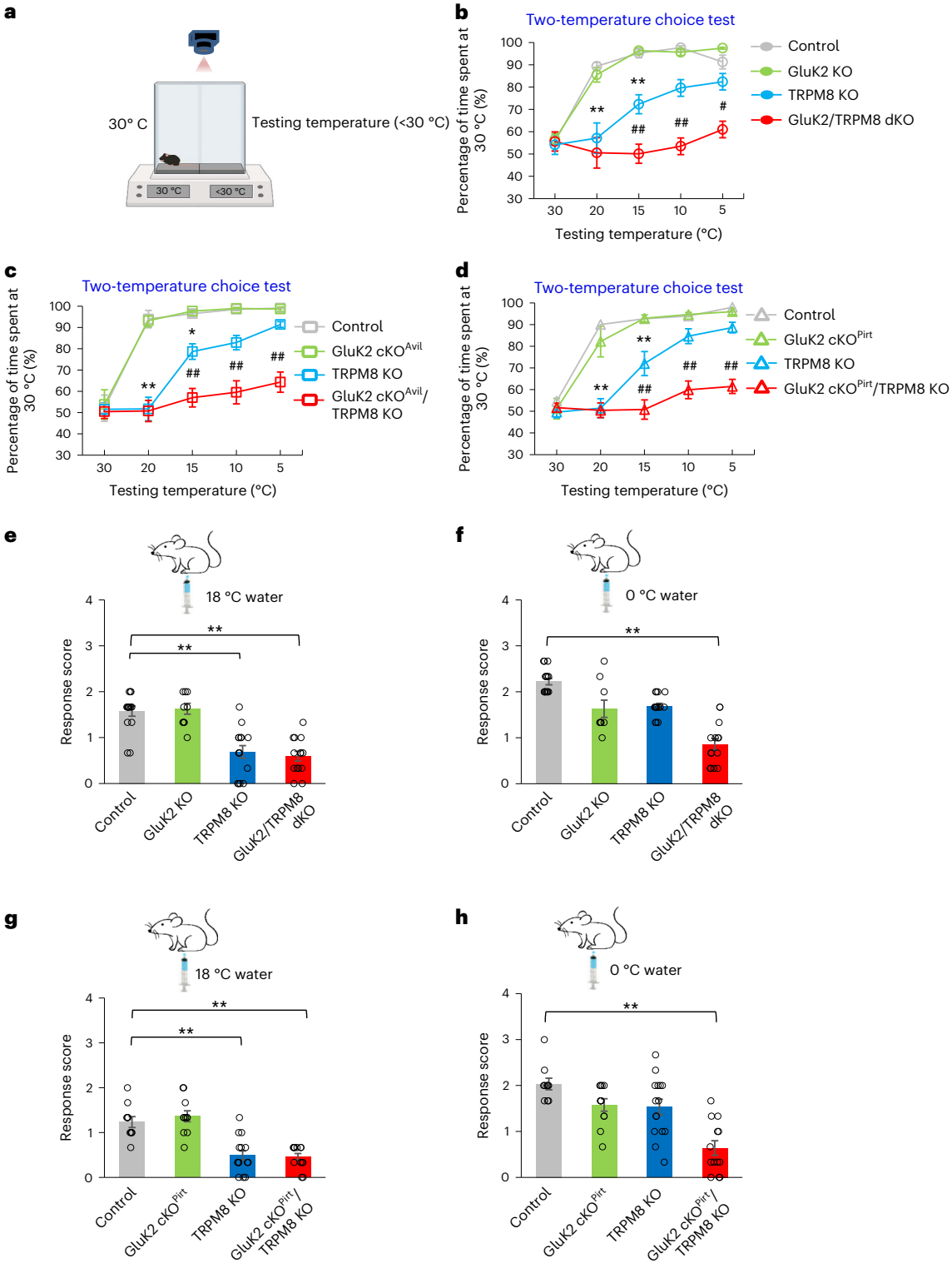

https://doi.org/10.1038/s41593-024-01585-8

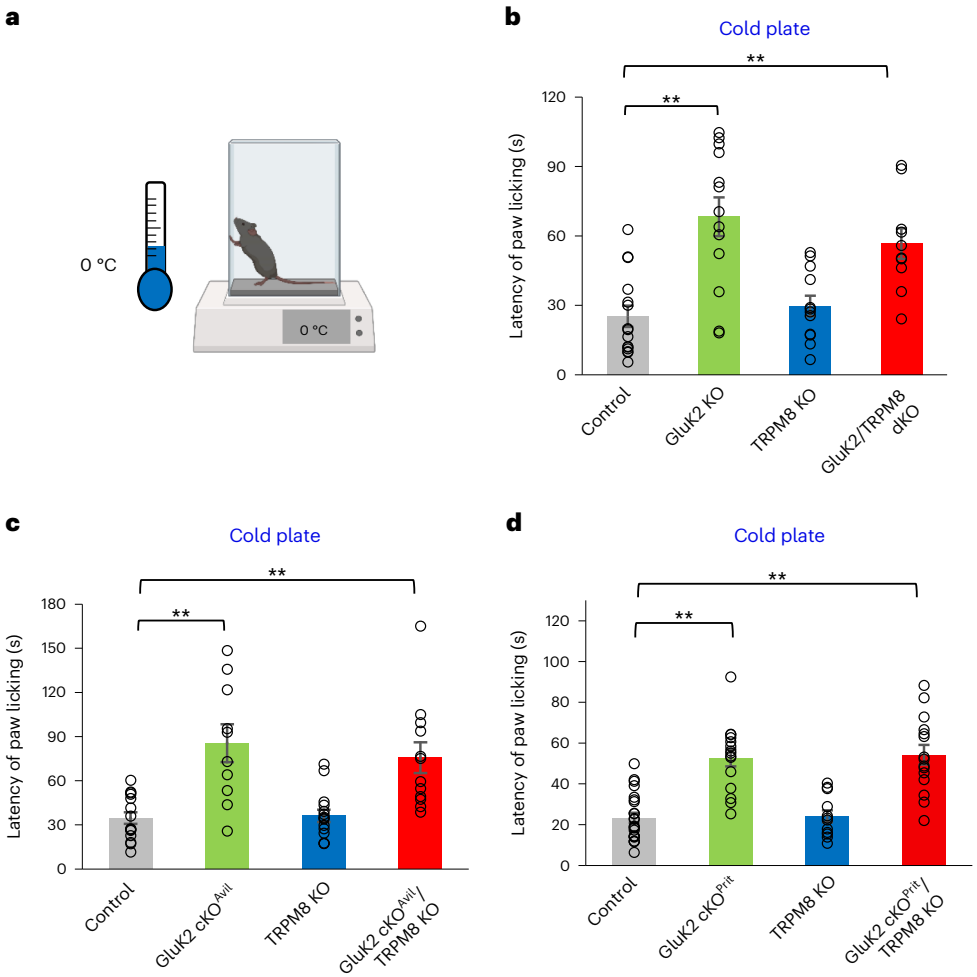

Fig. 3 | GluK2 KO mice are defective in cold nociception. a, Schematic diagram of the cold-plate assay. **b**, GluK2 KO mice are defective in cold nociception as shown by the cold-plate assay. The latency of forepaw licking was quantified. Error bars, s.e.m. Sample size: control $n = 15$, GluK2 KO $n = 13$, TRPM8 KO $n = 12$, GluK2/TRPM8 dKO $n = 10$. $^{**}P = 2.7 \times 10^{-5}$ (GluK2 KO versus control), $^{**}P = 0.0053$ (GluK2/TRPM8 dKO versus control), one-way ANOVA with Tukey's test. **c**, GluK2 cKO^{Avil} mice are defective in cold nociception as shown by the cold-plate assay. An Avil-Cre line was used to selectively ablate GluK2 from DRG neurons. The latency of forepaw licking was quantified. Error bars, s.e.m. Sample size: control $n = 15$, GluK2 cKO^{Avil} $n = 10$, TRPM8 KO $n = 15$, GluK2 cKO^{Avil}/TRPM8 dKO $n = 12$. $^{**}P = 0.00022$ (GluK2 cKO^{Avil} versus control), $^{**}P = 0.0019$ (GluK2 cKO^{Avil}/TRPM8 dKO versus control), one-way ANOVA with Tukey's test. **d**, GluK2 cKO^{Pirt} mice are defective in cold nociception as shown by the cold-plate assay. A Pirt-Cre line was used to selectively ablate GluK2 from DRG neurons. The latency of forepaw licking was quantified. Error bars, s.e.m. Sample size: control $n = 23$, GluK2 cKO^{Pirt} $n = 15$, TRPM8 KO $n = 12$, GluK2 cKO^{Pirt}/TRPM8 dKO $n = 15$. $^{**}P = 4.8 \times 10^{-7}$ (GluK2 cKO^{Pirt} versus control), $^{**}P = 1.6 \times 10^{-7}$ (GluK2 cKO^{Pirt}/TRPM8 dKO versus control), one-way ANOVA with Tukey's test. Note: all data are presented as mean ± s.e.m. Wild-type and heterozygous littermate mice were used as the controls in all panels. Both male and female mice were assayed, except in **c** where only male mice were selected for testing because of a germline-leak concern in Avil-Cre female mice. No significant difference between males and females was observed in the behavioral assays (Supplementary Fig. 3).

defect when challenged by such cold stimuli (Fig. 2f, Supplementary Fig. 2d and Supplementary Table 1), unveiling an important role for GluK2 in sensing cold temperatures. This set of data, together with those described above, uncovers a rather specific function of GluK2 in sensing cold but not cool, heat or mechanical stimuli.

GluK2 KO mice are defective in cold nociception

The observation that GluK2 is important for mice to sense cold temperatures prompted us to ask whether GluK2 contributes to cold nociception. As both the two-temperature choice assay and paw withdrawal assay are better suited for testing threshold-level thermal discrimination and avoidance rather than nociception[18], we performed the cold-plate assay which is commonly used to examine cold nociception[19]. To do so, we assayed cold-induced repetitive paw-licking responses evoked by sustained exposure to a 0 °C cold plate[19] (Fig. 3a). Consistent with previous reports[6,7], TRPM8 KO mice did not show a defect in the cold-plate assay (Fig. 3b and Supplementary Fig. 3a), supporting the notion that the cool sensor TRPM8 does not play a major role in mediating cold nociception. By contrast, GluK2 KO mice displayed a strong defect in cold nociception (Fig. 3b and Supplementary Fig. 3a), and a similar defect was observed in GluK2/TRPM8 dKO mice (Fig. 3b and Supplementary Fig. 3a). Thus, GluK2 is not only important for mice to sense cold temperatures but also mediates cold nociception.

Mick lacking GluK2 in DRG neurons are cold-sensing defective

In addition to the central nervous system, GluK2 is expressed in DRG neurons[20]. We thus wondered if the observed cold-sensing phenotypes in GluK2 KO mice resulted from a defect in DRG neurons. To address this question, we conditionally knocked out GluK2 from DRG neurons using two independent Cre lines: Avil-Cre and Pirt-Cre[21,22]. As a control, we first examined the heat and mechanical sensitivity of GluK2 conditional knockout (cKO) mice. We found that GluK2 cKO^{Avil} and GluK2 cKO^{Pirt} mice, as well as GluK2 cKO^{Avil}/TRPM8 KO and GluK2 cKO^{Pirt}/TRPM8 KO mice, all responded normally to heat and mechanical stimuli (Extended

https://doi.org/10.1038/s41593-024-01585-8

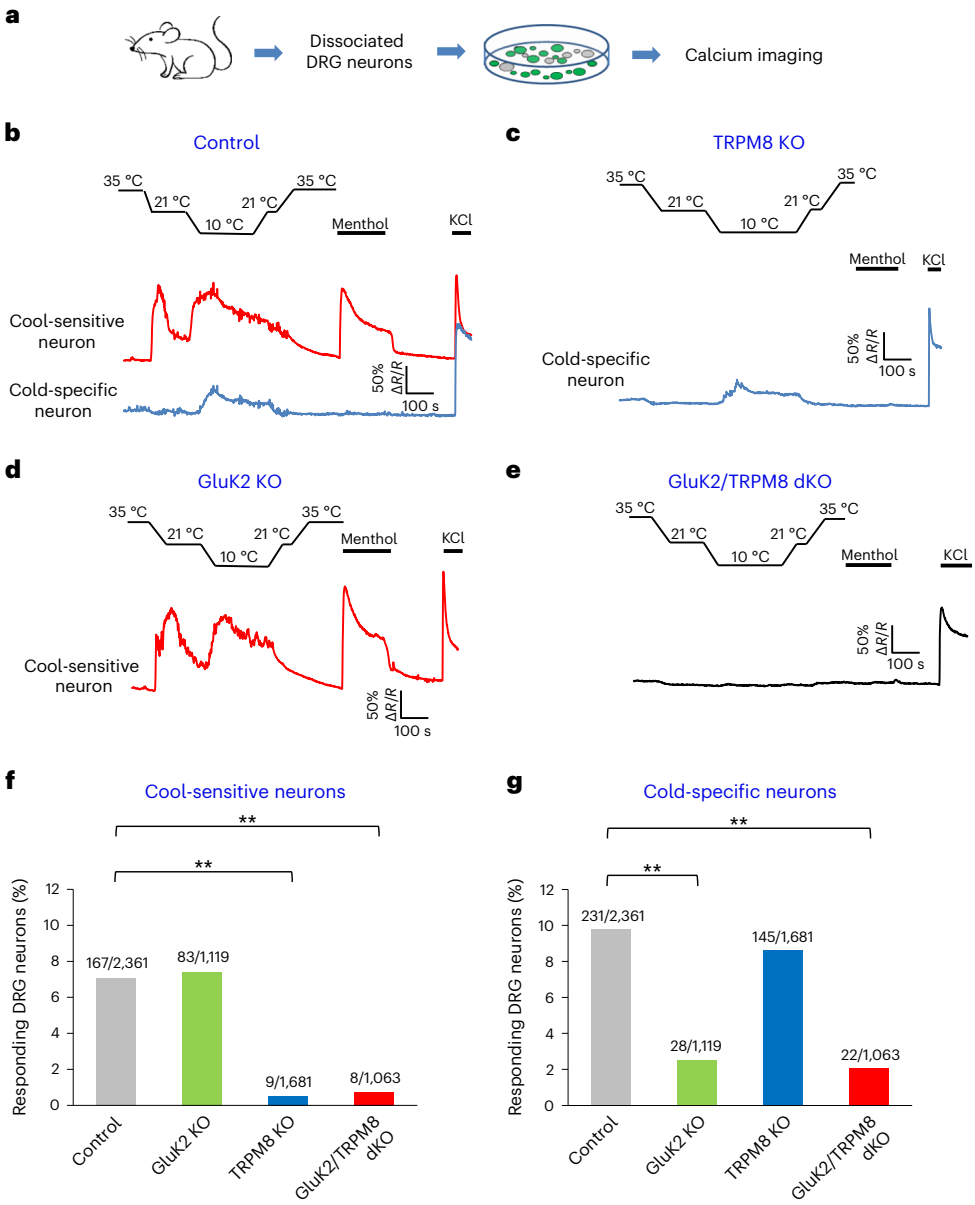

Fig. 4 | Calcium imaging reveals that GluK2 is important for sensing cold rather than cool temperatures in dissociated DRG neurons. a, Schematic description of the assay. **b**–**e**, Sample traces of cool-sensitive and cold-specific DRG neurons. **b**, Control: DRG neurons isolated from wild-type littermate mice. **c**, TRPM8 KO. **d**, GluK2 KO. **e**, GluK2/TRPM8 dkO. Dissociated DRG neurons were recorded for their responses to temperature stimuli by calcium imaging. The temperature stimulus protocol is indicated on the top. Menthol: 100 μM. KCl: 50 mM. **f**, KO of GluK2 does not affect the cool-sensitive DRG neuron population, though these neurons are nearly eliminated by KO of TRPM8. Control: DRG neurons isolated from wild-type littermate mice. The numbers of responding neurons and total neurons assayed are listed. $^{**}P = 1 \times 10^{-10}$ (TRPM8 KO versus control group), $^{**}P = 5.2 \times 10^{-7}$ (GluK2/TRPM8 dKO versus control group), chi-squared test. **g**, KO of GluK2 but not TRPM8 greatly reduces the cold-specific DRG neuron population. Control: DRG neurons isolated from wild-type littermate mice. The numbers of responding neurons and total neurons assayed are listed. The number of mice used to isolate DRG neurons in **f** and **g**: control (31 mice), TRPM8 KO (19 mice), GluK2 KO (15 mice), GluK2/TRPM8 dKO (10 mice). $^{**}P = 4.7 \times 10^{-7}$ (GluK2 KO versus control group), $^{**}P = 5.2 \times 10^{-7}$ (GluK2/TRPM8 dKO versus control group), chi-squared test.

Data Figs. 2 and 3), a result similar to that obtained with whole-body KO mice. Notably, as was the case with whole-body KO mice, GluK2 cKO^{Pirt}/TRPM8 KO and GluK2 cKO^{Avil}/TRPM8 KO mice manifested a strong defect in sensing cold temperatures in the two-temperature choice assay (Fig. 2c,d and Supplementary Fig. 2b). Similarly, a strong defect was found in GluK2 cKO^{Pirt}/TRPM8 KO mice in sensing cold temperatures in the paw withdrawal assay (Fig. 2g,h, Supplementary Fig. 2e,f and Supplementary Table 1). As observed in whole-body KO mice, both GluK2 cKO^{Avil} and GluK2 cKO^{Pirt} mice were also defective in cold nociception in the cold-plate assay (Fig. 3c,d and Supplementary Fig. 3b). This set of data demonstrates that selective deletion of GluK2 from DRG neurons led to similar cold-sensing phenotypes, suggesting that GluK2 can function in the DRG to mediate cold sensing in mice.

GluK2 is important for DRG neurons to sense cold in vitro

Having identified an important role for GluK2 in mediating cold sensing at the behavioral level, we then sought to characterize the underlying neuronal mechanisms. To do so, we dissociated DRG neurons and recorded their responses to cooling by calcium imaging (Fig. 4a). As previously reported[6], we identified two major types of cooling-activated DRG neurons. The first group can be activated by cool temperature stimuli (cooling to room temperature at 21 °C) (Fig. 4b

https://doi.org/10.1038/s41593-024-01585-8

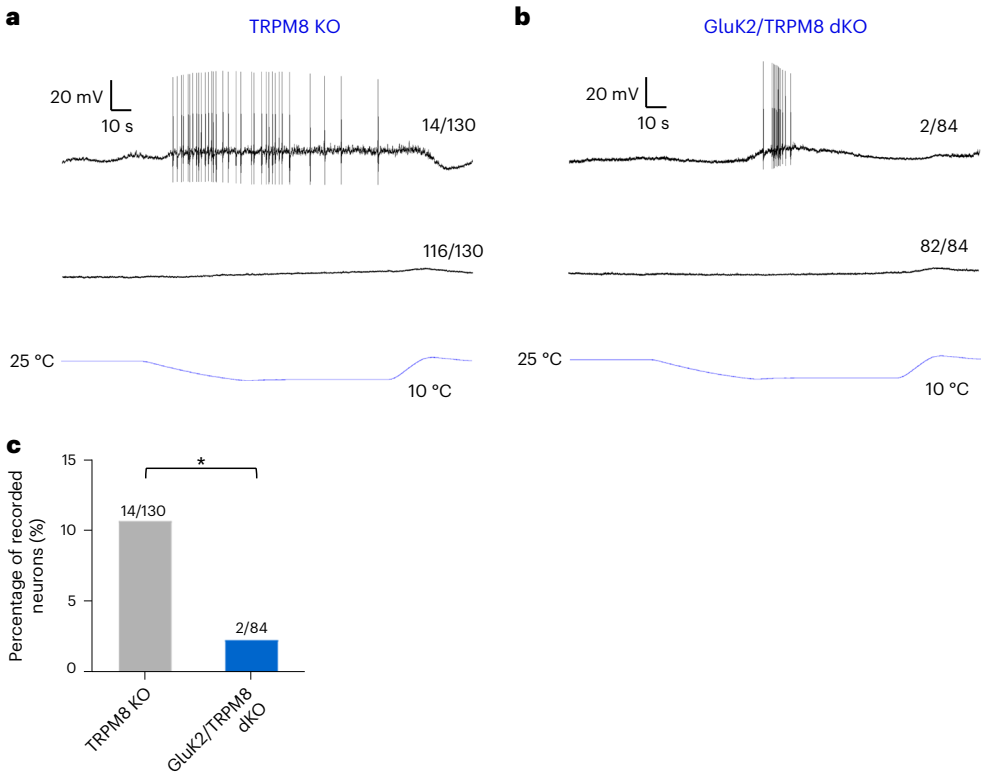

Fig. 5 | Patch-clamp recording reveals that GluK2 is important for cold sensing in dissociated DRG neurons. a, Sample traces of cold-evoked AP firing in DRG neurons isolated from TRPM8 KO mice. The numbers of responding and nonresponding neurons and total neurons recorded are indicated. **b**, Sample traces of cold-evoked AP firing in DRG neurons isolated from GluK2/TRPM8 dKO mice. The numbers of responding and nonresponding neurons and total neurons recorded are indicated. **c**, The percentage of cold-activated DRG neurons is greatly reduced in GluK2/TRPM8 dKO mice compared with TRPM8 KO mice. Bar graph summarizing the data in **a** and **b**. The numbers of responding neurons and total neurons recorded are listed. The numbers of mice used to isolate DRG neurons: TRPM8 KO (11 mice), GluK2/TRPM8 dKO (6 mice). Error bars, s.e.m. *P = 0.023 (GluK2/TRPM8 dKO versus TRPM8 KO group), chi-squared test.

and Extended Data Figs. 4 and 5), though deeper cooling to the cold range (10 °C) can also activate this type of DRG neurons (Fig. 4b and Extended Data Fig. 4a). These neurons were sensitive to menthol, suggesting that they are TRPM8$^+$ neurons (Fig. 4b and Extended Data Fig. 4a). We thus named them cool-sensitive neurons. A second group of cooling-activated DRG neurons possessed a relatively higher activation threshold, as they were insensitive to cool temperatures and can only be activated by cold temperatures (Fig. 4b and Extended Data Fig. 4a). Unlike cool-sensitive neurons, these neurons were insensitive to menthol (Fig. 4b and Extended Data Fig. 4a). We thus named them cold-specific neurons. Both cool-sensitive and cold-specific neurons showed little or no sensitivity to AITC (Extended Data Fig. 6a,b), an agonist of TRPA1 that plays an important role in sensing hot temperatures in DRG neurons[3]. In TRPM8 KO mice, cool-sensitive neurons were largely absent (Fig. 4c,f and Extended Data Figs. 4 and 5), suggesting that their cool sensitivity is mediated by TRPM8. As expected, the population of cool-sensitive neurons remained intact in GluK2 KO mice (Fig. 4d,f and Extended Data Figs. 4 and 5), supporting the notion that GluK2 does not contribute to cool sensing. Notably, the cold-specific neuron population remained intact in TRPM8 KO mice (Fig. 4c,g and Extended Data Figs. 4 and 5), indicating that TRPM8 does not contribute to the cold sensitivity of cold-specific neurons. Strikingly, while the loss of GluK2 did not affect the population of cool-sensitive neurons (Fig. 4d,f and Extended Data Figs. 4 and 5), the cold-specific neuron population was greatly reduced in the DRG culture prepared from GluK2 KO mice (Fig. 4d,g and Extended Data Figs. 4 and 5), revealing a specific function for GluK2 in mediating cold rather than cool sensing in DRG neurons.

We also identified a small population (~3% of DRG neurons) of a third type of cooling-activated DRG neurons that were sensitive to menthol but unresponsive to cool temperature stimuli, though they can be activated by cold temperatures (Extended Data Fig. 7a). These menthol-sensitive neurons were not affected by GluK2 deletion but were nearly absent in TRPM8 KO mice (Extended Data Fig. 7a), indicating that they were also TRPM8$^+$ neurons. A similar phenomenon has been reported previously[23], but it is unclear exactly why these TRPM8$^+$ neurons were insensitive to cool temperature stimuli; nevertheless, due to their small population size and independence of GluK2, we did not further characterize these neurons.

Notably, in GluK2/TRPM8 dKO mice, both the cool-sensitive and cold-specific neuron populations were greatly decreased (Fig. 4e–g and Extended Data Figs. 4 and 5). Thus, it appears that the majority of cooling-activated neurons in the DRG depend on GluK2 and TRPM8. Together, this set of experiments unveil a specific role for GluK2 in sensing cold rather than cool temperatures in dissociated DRG neurons.

To obtain additional evidence supporting a role for GluK2 in cold sensing, we recorded dissociated DRG neurons by whole-cell patch-clamp recording. To facilitate the identification of cold-specific neurons, we focused on patching DRG neurons isolated from TRPM8 KO mice, as these mice lack cool-sensitive neurons in the DRG. We found that cold stimuli triggered action potential (AP) firing in ~11% (14 of 130) of DRG neurons isolated from TRPM8 KO mice (Fig. 5a,c). Importantly, the percentage of such cold-activated DRG neurons was reduced to ~2.4% (2 of 84) in GluK2/TRPM8 dKO mice (Fig. 5b,c), uncovering an important role of GluK2 in mediating cold sensing in DRG neurons. As a control, we detected no notable difference in the intrinsic excitability and other electrical properties of DRG neurons between TRPM8 KO and GluK2/TRPM8 dKO mice (Extended Data Fig. 8), indicating that loss of GluK2

https://doi.org/10.1038/s41593-024-01585-8

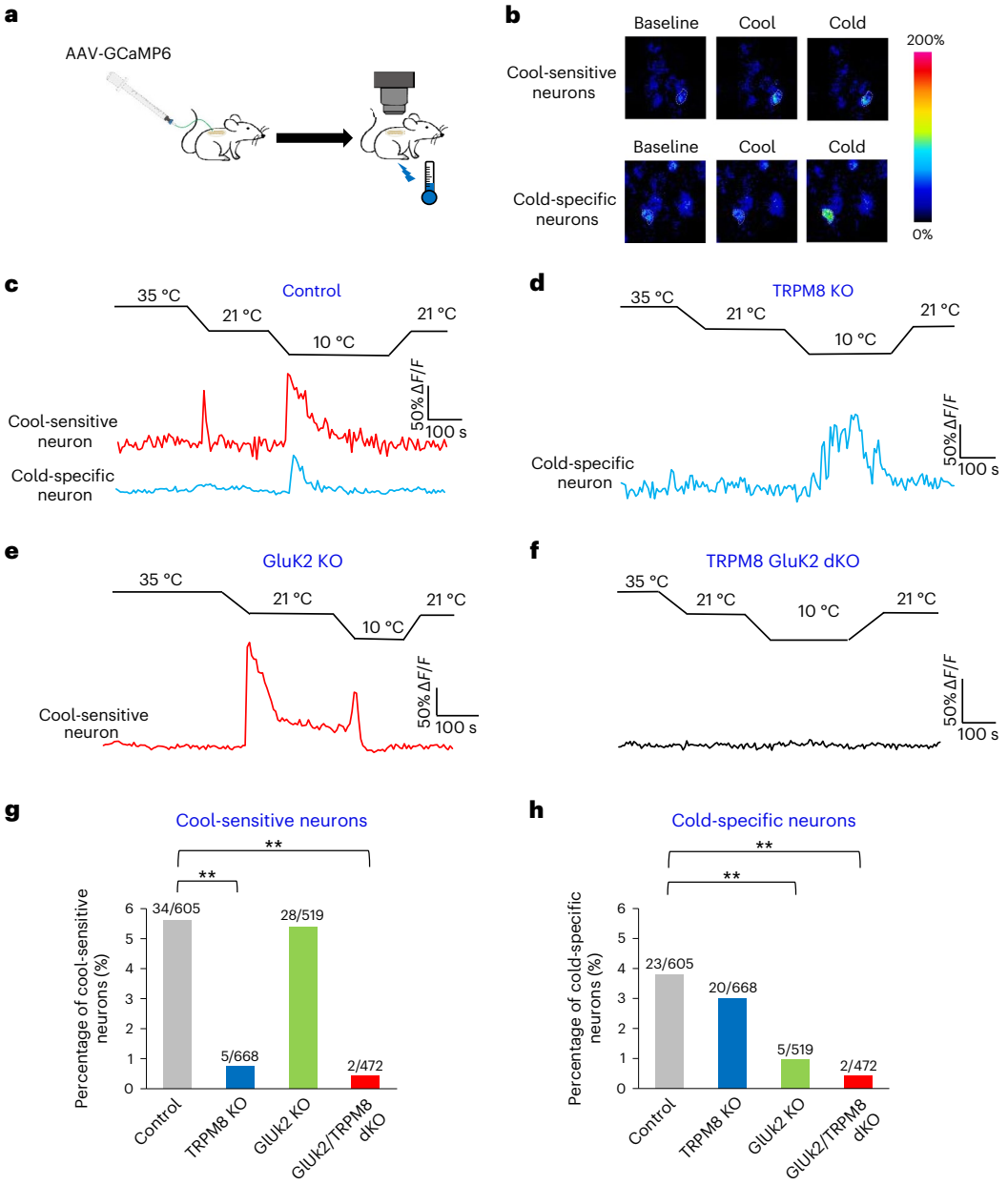

Fig. 6 | GluK2 is important for sensing cold rather than cool temperatures in DRG neurons in vivo. a, Schematic description of the assay. GCaMP6 was expressed in DRG neurons by intrathecal injection of AAV9-GCaMP6 viruses into the subarachnoid space near L5. L5 DRG neurons were imaged for responses to temperature stimuli applied to the hindpaw. **b**, Sample images of cool-sensitive and cold-specific DRG neurons. Shown are snapshot pseudocolor images of DRG neurons in response to cool and cold temperature stimuli. Pseudocolors refer to relative calcium levels in the neuron. Five mice were recorded. **c**–**f**, Sample traces of cool-sensitive and cold-specific DRG neurons. **c**, Control: wild-type and heterozygous littermate mice. **d**, TRPM8 KO mice. **e**, GluK2 KO mice. **f**, GluK2/TRPM8 dKO mice. The temperature stimulus protocol is shown on the top. **g**, The cool-sensitive DRG neuron population is not affected in GluK2 KO mice but is nearly eliminated in TRPM8 KO and GluK2/TRPM8 dKO mice. Control: wild-type and heterozygous littermate mice. The numbers of responding neurons and total neurons assayed are listed. Five mice in each group. $^{**}P = 4.7 \times 10^{-7}$ (TRPM8 KO versus control), $^{**}P = 2.5 \times 10^{-6}$ (GluK2/TRPM8 dKO versus control group), chi-squared test. **h**, The cold-specific DRG neuron population is greatly reduced in GluK2 KO mice and GluK2/TRPM8 dKO mice but is not notably affected in TRPM8 KO mice. Control: wild-type and heterozygous littermate mice. The numbers of responding neurons and total neurons assayed are listed. Five mice in each group. $^{**}P = 0.0023$ (GluK2 KO versus control group), $^{**}P = 0.00026$ (GluK2/TRPM8 dKO versus control group), chi-squared test.

did not affect the overall health of DRG neurons. These recordings provide further evidence supporting a role for GluK2 in sensing cold temperatures in dissociated DRG neurons, unveiling a neuronal mechanism underlying the observed cold-sensing behavioral phenotypes in GluK2 KO mice.

GluK2 is important for DRG neurons to sense cold in vivo

To provide further evidence, we set out to record the activity of DRG neurons in response to cooling by in vivo calcium imaging using a protocol as previously described[24–26]. To do so, we expressed GCaMP6, a genetically encoded calcium sensor, in DRG neurons by intrathecal injection of AAV9-GCaMP6 viruses into mice (Fig. 6a). Similar to the case with dissociated DRG neurons cultured in vitro, we also detected two distinct classes of cooling-activated DRG neurons, cool-sensitive neurons and cold-specific neurons, when imaging the DRG in vivo (Fig. 6b,c and Extended Data Fig. 9a). Specifically, application of cool temperature stimuli (cooling to 21 °C) to the mouse paw was sufficient to activate cool-sensitive DRG neurons (Fig. 6c and

Extended Data Fig. 9a). Similarly, deeper cooling to the cold range (10 °C) can also activate these neurons (Fig. 6c and Extended Data Fig. 9a). By contrast, cold-specific DRG neurons possessed a higher activation threshold, as they were unresponsive to cool temperatures and can only be turned on by cold temperature stimuli (Fig. 6c and Extended Data Fig. 9a). Knocking out TRPM8 nearly eliminated cool-sensitive neurons while leaving the population of cold-specific neurons unchanged (Fig. 6d,g,h and Extended Data Fig. 9), supporting the notion that TRPM8 is required for DRG neurons to sense cool but not cold temperatures. By contrast, GluK2 ablation led to a severe reduction in cold-specific neurons while having no significant effect on the cool-sensitive neuron population (Fig. 6e,g,h and Extended Data Fig. 9), uncovering a specific role for GluK2 in mediating cold sensing in DRG neurons in vivo. Lastly, dKO of GluK2 and TRPM8 greatly reduced the population of both cool-sensitive and cold-specific DRG neurons (Fig. 6f–h and Extended Data Fig. 9). These results provide a neuronal basis for the cold-sensing behavioral phenotypes observed in GluK2 KO mice.

Discussion

Animals and humans are capable of sensing a wide range of temperature cues, spanning from cold, cool and warm to hot temperatures[1,2]. The identification of a large number of temperature-sensitive TRP channels as molecular thermosensors detecting cool, warm and hot temperatures has greatly advanced our understanding of cool, warm and hot sensing[1]. By contrast, much less is known about cold sensing, largely due to the lack of a molecular understanding of thermosensors specialized in sensing cold temperatures[1,8]. In the current study, by characterizing GluK2 KO mice, we provided multiple lines of evidence uncovering a key role of GluK2 in cold sensing. Our results demonstrate that GluK2 mediates cold sensing in mice, supporting GluK2 as a cold sensor.

The role of GluK2 in cold sensing appears rather specific, as GluK2 KO mice respond normally to mechanical and heat stimuli. GluK2 KO mice also lack a phenotype in cool sensing, which is further supported by DRG neuron recordings performed both in vitro and in vivo. A specific role of GluK2 in sensing cold but not cool temperatures is consistent with its relatively high activation threshold compared with that of the cool sensor TRPM8, indicating that GluK2 and TRPM8 can function independently of each other in the DRG. This is also consistent with the finding that GluK2 and TRPM8 transcripts are detected in distinct groups of DRG neurons (refs. 15,16 and Extended Data Fig. 10). Nevertheless, it remains possible that GluK2 and TRPM8 may function together in a small DRG population, as a low percentage of DRG neurons coexpress GluK2 and TRPM8 (refs. 15,16 and Extended Data Fig. 10). Though TRPM8 is classified as a cool sensor, it can also be activated by cold temperatures and participates in cold sensing along with GluK2. Whether and how GluK2 interacts with TRPM8 at the cellular and/or circuit levels to mediate cold sensing requires further investigation. Lastly, while GluK2 appears to be a major contributor to cold sensing in DRG neurons, we do not exclude the possibility that additional cold sensors may exist, given the presence of residual cold responses in GluK2/TRPM8 dKO mice. One possibility is that other proposed cold sensors, such as TRPA1, TRPC5, K2P and Orai channels[8,27–29], might play a role; alternatively, an unknown cold sensor(s) might be involved.

One interesting observation is that GluK2 KO but not TRPM8 KO mice are defective in cold nociception. While the absence of a notable phenotype in cold nociception in TRPM8 KO mice is expected, the presence of such a deficit in GluK2 KO mice is rather surprising, considering that TRPM8 would be expected to sense cold in GluK2 KO mice. On the other hand, cold nociception (paw-licking behavior) represents a typical interoceptive self-caring response to body injury, which is distinct from those threshold-level cold avoidance/discrimination behaviors that are considered reflex responses and likely require distinct circuit mechanisms in the spinal and brain regions[18]. This might explain the observed cold nociception phenotype in GluK2 KO mice. Exposure to cold, particularly chronic cold, causes tissue damage and evokes pain[30,31]. Cold-induced pain represents a severe health condition[30,31]. Currently, there are no effective cures for cold pain[30,31]. Our study identifies GluK2 as a new drug target for developing therapeutics treating cold pain.

GluK2 is known to possess both ionotropic and metabotropic functions[32,33]. In the central nervous system, GluK2 primarily functions as an ionotropic glutamate-sensing chemoreceptor transmitting synaptic glutamate signals[9,34]. In the DRG, our data suggest that GluK2 can act as a cold-sensing thermoreceptor. Interestingly, GluK2 relies on its metabotropic rather than ionotropic function for cold sensing in vitro by transmitting cold signals via G protein signaling, particularly Gi/o signaling[10]. Specifically, the cold-sensing function of GluK2, when expressed in heterologous systems, is not affected by mutations that ablate its channel activity, but instead can be blocked by the Gi/o inhibitor pertussis toxin[10]. In dissociated DRG neurons, we found that the percentage of cold-specific neurons but not cool-sensitive neurons was greatly reduced by pertussis toxin treatment (Extended Data Fig. 6c–e), suggesting that a similar metabotropic mechanism may underlie the function of GluK2 in cold sensing in DRG neurons. Thus, GluK2 may represent a novel non-channel type of thermosensor. How GluK2 transmits cold signals via G protein signaling to regulate neuronal excitability is currently unknown. Presumably, opening/closing of a downstream transduction channel(s) might be involved. It should be noted that over 20% of DRG neurons express GluK2 transcripts (Extended Data Fig. 10c), which is considerably higher than that of cold-specific neurons in the DRG. One possibility is that some GluK2$^+$ DRG neurons might lack certain key components that act downstream of GluK2 to transmit cold signals; alternatively, such neurons might express some genes that inhibit the cold-sensing function of GluK2. Future studies are needed to elucidate the detailed signaling pathway by which GluK2 transmits cold signals. Evolutionarily, it remains a mystery as to how an ionotropic chemosensor in the central nervous system is co-opted as a metabotropic thermosensor in the periphery. Notably, iGluRs form an ancient gene family present in nearly every organism including bacteria[9]. Perhaps, some iGluRs (for example, GluK2) are multifunctional, capable of sensing chemicals as well as other cues such as temperature. Notably, most thermosensitive TRP channels (for example, TRPV1, TRPM2, TRPM3 and TRPM8) are only found in vertebrates but are absent in invertebrates[1,35,36]. In addition, for those thermosensitive TRPs that are present in both vertebrate and invertebrate genomes (for example, TRPA1), their temperature-sensing function tends to diverge across phyla[1,35,36]; for example, TRPA1 is a heat sensor in insects and snakes, but acts as a cold sensor in nematodes[37–41]. Unlike thermosensitive TRP channels, homologs of GluK2 exist in both vertebrate and invertebrate species[9], and, importantly, they all can function as cold sensors at least in vitro[10]. We thus propose that GluK2 represents an ancient class of evolutionarily conserved thermosensor.

Online content

Any methods, additional references, Nature Portfolio reporting summaries, source data, extended data, supplementary information, acknowledgements, peer review information; details of author contributions and competing interests; and statements of data and code availability are available at https://doi.org/10.1038/s41593-024-01585-8.

References

1. Xiao, R. & Xu, X. Z. S. Temperature sensation: from molecular thermosensors to neural circuits and coding principles. *Annu. Rev. Physiol.* **83**, 205–230 (2021).

2. Palkar, R., Lippoldt, E. K. & McKemy, D. D. The molecular and cellular basis of thermosensation in mammals. *Curr. Opin. Neurobiol.* **34**, 14–19 (2015).
3. Vandewauw, I. et al. A TRP channel trio mediates acute noxious heat sensing. *Nature* **555**, 662–666 (2018).
4. Tan, C. H. & McNaughton, P. A. The TRPM2 ion channel is required for sensitivity to warmth. *Nature* **536**, 460–463 (2016).
5. Song, K. et al. The TRPM2 channel is a hypothalamic heat sensor that limits fever and can drive hypothermia. *Science* **353**, 1393–1398 (2016).
6. Bautista, D. M. et al. The menthol receptor TRPM8 is the principal detector of environmental cold. *Nature* **448**, 204–208 (2007).
7. Dhaka, A. et al. TRPM8 is required for cold sensation in mice. *Neuron* **54**, 371–378 (2007).
8. Buijs, T. J. & McNaughton, P. A. The role of cold-sensitive ion channels in peripheral thermosensation. *Front. Cell. Neurosci.* **14**, 262 (2020).
9. Traynelis, S. F. et al. Glutamate receptor ion channels: structure, regulation, and function. *Pharm. Rev.* **62**, 405–496 (2010).
10. Gong, J. et al. A cold-sensing receptor encoded by a glutamate receptor gene. *Cell* **178**, 1375–1386 e1311 (2019).
11. Fujita, F., Uchida, K., Takaishi, M., Sokabe, T. & Tominaga, M. Ambient temperature affects the temperature threshold for TRPM8 activation through interaction of phosphatidylinositol 4,5-bisphosphate. *J. Neurosci.* **33**, 6154–6159 (2013).
12. McKemy, D. D., Neuhausser, W. M. & Julius, D. Identification of a cold receptor reveals a general role for TRP channels in thermosensation. *Nature* **416**, 52–58 (2002).
13. Peier, A. M. et al. A TRP channel that senses cold stimuli and menthol. *Cell* **108**, 705–715 (2002).
14. Bandell, M., Macpherson, L. J. & Patapoutian, A. From chills to chilis: mechanisms for thermosensation and chemesthesis via thermoTRPs. *Curr. Opin. Neurobiol.* **17**, 490–497 (2007).
15. Usoskin, D. et al. Unbiased classification of sensory neuron types by large-scale single-cell RNA sequencing. *Nat. Neurosci.* **18**, 145–153 (2015).
16. Sharma, N. et al. The emergence of transcriptional identity in somatosensory neurons. *Nature* **577**, 392–398 (2020).
17. Duan, B. et al. Identification of spinal circuits transmitting and gating mechanical pain. *Cell* **159**, 1417–1432 (2014).
18. Ma, Q. A functional subdivision within the somatosensory system and its implications for pain research. *Neuron* **110**, 749–769 (2022).
19. Knowlton, W. M. et al. A sensory-labeled line for cold: TRPM8-expressing sensory neurons define the cellular basis for cold, cold pain, and cooling-mediated analgesia. *J. Neurosci.* **33**, 2837–2848 (2013).
20. Mulle, C. et al. Altered synaptic physiology and reduced susceptibility to kainate-induced seizures in GluR6-deficient mice. *Nature* **392**, 601–605 (1998).
21. Zhou, X. et al. Deletion of PIK3C3/Vps34 in sensory neurons causes rapid neurodegeneration by disrupting the endosomal but not the autophagic pathway. *Proc. Natl Acad. Sci. USA* **107**, 9424–9429 (2010).
22. Han, L. et al. Mrgprs on vagal sensory neurons contribute to bronchoconstriction and airway hyper-responsiveness. *Nat. Neurosci.* **21**, 324–328 (2018).
23. Sarria, I., Ling, J., Xu, G. Y. & Gu, J. G. Sensory discrimination between innocuous and noxious cold by TRPM8-expressing DRG neurons of rats. *Mol. Pain* **8**, 79 (2012).
24. Kim, Y. S. et al. Coupled activation of primary sensory neurons contributes to chronic pain. *Neuron* **91**, 1085–1096 (2016).
25. Emery, E. C. et al. In vivo characterization of distinct modality-specific subsets of somatosensory neurons using GCaMP. *Sci. Adv.* **2**, e1600990 (2016).
26. Wang, F. et al. Sensory afferents use different coding strategies for heat and cold. *Cell Rep.* **23**, 2001–2013 (2018).
27. Story, G. M. et al. ANKTM1, a TRP-like channel expressed in nociceptive neurons, is activated by cold temperatures. *Cell* **112**, 819–829 (2003).
28. Buijs, T. J., Vilar, B., Tan, C. H. & McNaughton, P. A. STIM1 and ORAI1 form a novel cold transduction mechanism in sensory and sympathetic neurons. *EMBO J.* **42**, e111348 (2022).
29. Zimmermann, K. et al. Transient receptor potential cation channel, subfamily C, member 5 (TRPC5) is a cold-transducer in the peripheral nervous system. *Proc. Natl Acad. Sci. USA* **108**, 18114–18119 (2011).
30. MacDonald, D. I., Wood, J. N. & Emery, E. C. Molecular mechanisms of cold pain. *Neurobiol. Pain* **7**, 100044 (2020).
31. Foulkes, T. & Wood, J. N. Mechanisms of cold pain. *Channels (Austin)* **1**, 154–160 (2007).
32. Rodriguez-Moreno, A. & Lerma, J. Kainate receptor modulation of GABA release involves a metabotropic function. *Neuron* **20**, 1211–1218 (1998).
33. Valbuena, S. & Lerma, J. Non-canonical signaling, the hidden life of ligand-gated ion channels. *Neuron* **92**, 316–329 (2016).
34. Lerma, J. Roles and rules of kainate receptors in synaptic transmission. *Nat. Rev. Neurosci.* **4**, 481–495 (2003).
35. Venkatachalam, K. & Montell, C. TRP channels. *Annu. Rev. Biochem.* **76**, 387–417 (2007).
36. Xiao, R. & Xu, X. Z. *C. elegans* TRP channels. *Adv. Exp. Med. Biol.* **704**, 323–339 (2011).
37. Viswanath, V. et al. Opposite thermosensor in fruitfly and mouse. *Nature* **423**, 822–823 (2003).
38. Gracheva, E. O. et al. Molecular basis of infrared detection by snakes. *Nature* **464**, 1006–1011 (2010).
39. Xiao, R. et al. A genetic program promotes *C. elegans* longevity at cold temperatures via a thermosensitive TRP channel. *Cell* **152**, 806–817 (2013).
40. Zhang, B. et al. Environmental temperature differentially modulates *C. elegans* longevity through a thermosensitive TRP channel. *Cell Rep.* **11**, 1414–1424 (2015).
41. Zhang, B. et al. Brain-gut communications via distinct neuroendocrine signals bidirectionally regulate longevity in *C. elegans*. *Genes Dev.* **32**, 258–270 (2018).

Methods

Animals

All animal experiments were performed in accordance with protocols approved by the Institutional Animal Care and Use Committee at the University of Michigan and Johns Hopkins University following National Institutes of Health (NIH) guidelines. All mouse lines were in the C57BL/6J background. Both male and female mice were used for all experiments, with the exception of mice containing Advillin-Cre, in which case only male mice were selected for testing due to a germline-leak concern in female mice. Mice were group housed at room temperature with ad libitum access to standard lab mouse pellet food and water on a 12-h light/12-h dark cycle. GluK2 KO mice were kindly provided by Susumu Tomita's laboratory at Yale University[20]. GluK2-floxed mice were kindly provided by Anis Contractor's laboratory at Northwestern University[42]. Pirt-Cre mice were generated previously[43]. Advillin-Cre mice were generated by Fan Wang's laboratory at Massachusetts Institute of Technology and were acquired from the Jackson Laboratory (no. 032536). TRPM8 KO mice were generated by David Julius's laboratory at University of California San Francisco and were acquired from the Jackson Laboratory (no. 008198).

Behavioral tests

All mice at 8–12 weeks of age were measured in a blinded manner. Mice were acclimatized to the behavioral testing equipment for 2–3 d before each test. After the 'habituation' session, acute somatosensory measures were recorded as described previously[17,44].

The rotarod assay. Mice were placed on the accelerating rotarod (IITC). The rotarod began at 4 r.p.m. and accelerated to 40 r.p.m. over 5 min. The time to fall was automatically recorded. The test was repeated three times at 20-min intervals and the average was calculated as rotarod latency.

Mechanical sensitivity tests. Mice were habituated in individual black plexiglass chambers with a mesh floor for 30 min for 3 consecutive days before the test. On the testing day, mechanical sensitivity was measured via three assays in the given order at 20-min intervals: (1) von Frey assay, (2) brush assay and (3) pinprick assay. (1) von Frey assay. The plantar surface of the mouse hindpaw was stimulated with calibrated von Frey monofilaments (0.008 g to 2 g, North Coast). The paw withdrawal threshold to the stimulation was determined by Dixon's up–down method[45]. (2) Brush assay. The hindpaw plantar was stimulated by gently stroking with a paintbrush (4-0) in the direction from heel to toe. The stimulation was performed ten times. Walking away or occasionally brief paw lifting (~1 s or less) following each stimulation was considered as a positive response. The test was repeated ten times at 1-min intervals, and the percentage of positive response was calculated. (3) Pinprick assay. The hindpaw plantar was stimulated with a pin without penetrating into the skin. Hindpaw lifting/flinching responses were considered as a positive response following each stimulation. The stimulation was performed ten times at 1-min intervals, and the percentage of positive response was calculated.

The Hargreaves test. Mice were habituated for 30 min in plastic boxes (IITC) on the glass floor for 3 d before the test. On the testing day, the mouse hindpaw plantar was exposed to a beam of radiant heat through a Hargraves device (IITC). The latency of paw withdrawal was recorded. The heat stimulation was repeated three times at 1-min intervals for each mouse, and the mean of the withdrawal latencies was calculated. A cutoff time of 30 s was set to prevent potential tissue damage.

The hot-plate/cold-plate tests. Mice were habituated on a temperature plate (IITC) at 22 °C (room temperature) for 10–15 min on 2 consecutive days. On the testing day, the temperature plate was set at 54 °C (hot) or 0 °C (cold). Mouse responses to temperatures were recorded by a camcorder (Sony). After the test, we went through the videos and calculated the latency of forepaw licking. To avoid tissue injury, a cutoff time was set at 30 s and 180 s for assays at 54 °C and 0 °C, respectively.

The two-temperature choice assay. Each of the two temperature plates (Bioseb) was set to the desired temperature. Mice were usually first tested using the hot- and cold-plate assays and then subjected to the two-temperature choice test. Mice were placed between the two plates, and their movements were tracked for 5 min via a camera controlled by a tracking software (Bioseb). The time spent on each plate during recording was analyzed to assess their thermal preference. As a first step, we tested each mouse to determine if it displayed a strong preference to either plate independently of temperature. To do so, we set both plates to 30 °C to assess if mice spent roughly 50% of their time on each side; however, some mice did not due to variations intrinsic to this assay, and those that spent more than 70% of their time on one plate were not included in further testing. Room humidity was maintained at 25–30%, as humidity affects the assay especially when the plate was cooled to cold temperatures, likely due to moisture accumulation on the plate. The same cohort of mice was assayed at all the temperatures for each genotype.

The temperature-controlled water droplet stimulation test. Mice were habituated in individual black plexiglass chambers with a mesh floor for 30 min on 2 consecutive days. On the testing day, following 30 min of habituation, a water droplet (20–25-µl volume) at a set temperature was applied to the plantar surface of the mouse hindpaw using a 2.5-ml syringe (Becton Dickinson) connected to a trimmed 200-µl pipette tip (inner diameter of the flat opening: ~2.5 mm). It is important to let the water droplet attached to the plantar for at least one second to allow enough time to cool down the plantar surface; otherwise, the test would be considered unsuccessful and reperformed 3 min later. Caution should be exercised to avoid directly touching the plantar surface with the pipette tip. The temperature of both the syringe and the water inside was carefully controlled by incubating the whole syringe in a water bath with a set temperature verified by a thermometer. The stimulation was performed three times at 3-min intervals. Each application was video-recorded for the first 2 min for subsequent analysis. The behavior in response to the temperature-controlled water stimulation was evaluated and scored: no response or simply walking away scored 0, a brief paw lifting scored 1, a paw flinch scored 2, multiple flinches or a paw lick scored 3, and repetitive paw licking and/or paw guarding scored 4.

DRG dissociation and calcium imaging of dissociated DRG neurons

Acute dissociation of DRG neurons. DRG neurons were acutely dissociated as described previously[44]. Mice at the age of 25–35 days postnatal were euthanized with CO_2. DRGs from T10 to L6 were collected in icy Ca^{2+}/Mg^{2+}-free Hanks' buffered salt solution (pH 7.0, Invitrogen). Collected DRGs were digested with papain (1.5 mg ml^{-1}, adjust pH to 7.0, Sigma) with 1 mg of L-Cys (Sigma) for 15–20 min at 37 °C. Digestion solution was then replaced with collagenase II and dispase II (6 mg ml^{-1}, Sigma) and incubated for 20–28 min at 37 °C. Following digestion, DRGs were gently triturated 8–10 times with a polished pipette. The cells were purified using a 70-µm filter (Falcon) and were centrifuged for 5 min at 1,000 r.p.m. to separate the cells from the supernatant. The cells were further resuspended in a neurobasal medium supplemented with 2% B27 supplement, 1% GlutaMAX, nerve growth factor (100 ng ml^{-1}) and glial cell line-derived neurotrophic factor (40 ng ml^{-1}) and then were plated on 13-mm coverslips that had been precoated with laminin and poly-D-lysine overnight and cultured for 1 h at 37 °C in an incubator. The medium was then replaced with fresh medium containing 2.5% FBS (Gibco) and cultured for 6 h before calcium imaging experiments.

Calcium imaging of dissociated DRG neurons. As previously described[44], DRG neurons were first incubated at 37 °C for 30 min in 4 µM Fura-2-acetoxymethyl ester with 0.2% Pluronic F127 (Thermo Fisher Scientific), and then rinsed with PBS buffer. DRG neurons were then incubated in standard extracellular solution (10 mM HEPES, 5 mM KCl, 140 mM NaCl, 2 mM $MgCl_2$, 2 mM $CaCl_2$ and 10 mM glucose, pH 7.4) for 15 min in an incubator. Calcium imaging was performed using a ×20 water-immersion objective with high transmission efficiency of ultraviolet light (Olympus IX73) under the excitation wavelengths 340 nm and 380 nm. A Hamamatsu Digital Camera C11440 was used for image acquisition, and images were processed with MetaFluor software (Molecular Devices). Menthol (100 µM) and KCl (50 mM) were dissolved in standard extracellular solution for use in the experiment. We used a bipolar In-line Cooler/Heater (SC-20 from Warner Instruments) to control the temperature of the recording solution. The temperature protocol was described in Fig. 4. Lastly, high KCl solution (50 mM) was perfused to DRG neurons to validate neuronal activity, and those neurons displaying a KCl response lower than a 0.5-fold increase in ratio ($\Delta R/R$) were considered unhealthy and not analyzed. Responding neurons were defined by the fluorescence ratio increase $\Delta R/R \geq 0.2$.

Whole-cell patch-clamp recording of dissociated DRG neurons

DRG neurons were dissociated as described above and cultured overnight for whole-cell patch-clamp recording. MultiClamp 700B amplifier and Axon Digidata 1550 digitizer (Axon Instruments) were used. Microelectrodes were pulled using borosilicate capillaries bearing filament (with inner diameter 0.86 mm, outer diameter 1.5 mm; World Precision Instruments) with a P-1000 pipette puller (Sutter Instruments). The resistance of the microelectrodes was 3–5 MΩ filled with pipette solution. After gigaseal formation, the whole-cell configuration was formed, then cell membrane capacitance and series resistance were compensated. The data were sampled at 10 kHz and low pass-filtered at 2 kHz with pClamp10.4 (Axon Instruments) and were analyzed with Clampfit 10.2 (Axon Instruments). The pipette solution contains (in mM): potassium gluconate 130, KCl 5, $MgCl_2$ 2, EGTA 5, HEPES 10, ATP·Na_2 5, $CaCl_2$ 1, and pH adjusted to 7.2 with KOH, 300–310 mOsm. The external solution contains (in mM): NaCl 140, KCl 5, $CaCl_2$ 2.5, $MgCl_2$ 1, HEPES 10, D-glucose 10, and pH adjusted to 7.2 with NaOH, 315–320 mOsm.

The intrinsic properties and excitability of DRG neurons were studied by injecting a family of current steps ranging from −20 to 100 pA in 10-pA increments with a duration of 1,000 ms. AP firing frequency was quantified as the number of APs per second. Rheobase was detected by the minimum current (in pA) required to evoke an AP. The voltage threshold was defined as the voltage (in mV) at which the AP initiated, and the threshold level was determined as the voltage point where the rapid increase in voltage occurred ($dV/dt > 15$ mV s^{-1}). The peak amplitude of APs (in mV) and half-width (in ms) were measured with the first AP appeared through event statistics.

To characterize cold temperature-evoked AP induction in DRG neurons, gap-free membrane potentials were recorded under current-clamp mode for a total of 6 min. The temperature of the bath solution was maintained and controlled by a temperature controller (CL-100, Warner Instruments) from 25 °C (1 min) to 10 °C (4 min) and back to 25 °C.

In vivo calcium imaging of DRG neurons

Intrathecal administration of Adeno-associated virus. Mice were anesthetized with 1.5–2% isoflurane and then placed on a heating pad to maintain the temperature around 35 °C. An incision was made on the back skin above the lumbar region, and a small cut was made on the intervertebral membrane between Lumbar 5 (L5) and L6 vertebrae (near the L5) to insert a small catheter of 0.2-mm diameter. Then, 5 µl of Adeno-associated virus (AAV) (pAAV9.CAG.GCaMP6s. WPRE. SV40, 2.5×10^{13} gc ml^{-1}, Addgene) was infused into the intrathecal space through a catheter.

DRG exposure surgery and in vivo calcium imaging. Mice were anesthetized with sodium pentobarbital (40–50 mg kg^{-1}). A dorsal laminectomy was performed from the spinal level L4 to L6, and only the transverse process of L5 was removed to expose the underlying L5 DRG while the vertebral plate over the spinal cord and dura was left intact. The surgery and imaging were performed as previously described[24]. During the surgery and imaging, mice were placed on a heating pad with a feedback-based system to maintain body temperature at 35 ± 0.5 °C as monitored by a rectal probe (DC temperature controller, FHC). Mice were kept anesthetized with 1.5–2% isoflurane (Anesthesia system, Harvard Apparatus) and placed on a microscope stage with the spinal column stabilized on a holder to avoid movement. The microscope stage was fixed under a laser-scanning confocal microscope (Leica), equipped with a macro-based, large-objective and fast EM-CCD camera. The live images were acquired at typically four frames with 600 Hz in frame-scan mode per 3 s (at depths below the dura from 0 to 70 µm, with a ×5, 0.5 numerical aperture macro dry objective at 512 × 512 pixel resolution). GCaMP6 was used as a highly sensitive calcium indicator of calcium transients in DRG neurons. For green fluorescence, solid diode lasers (Leica) were used (excitation at 488 nm and emission at 500–549 nm).

The L5 whole DRG was placed at the focal plane, and images were recorded while applying thermal stimulation to the right hindpaw of the mouse. The hindpaw was stabilized in a custom-designed stimulation container, and water at the adaptation temperature was infused into the container at an average flow rate as previously described[46]. The water temperature was monitored and adjusted using a thermometer. Before each trial, images were recorded for 30–60 s without water stimulation to obtain baseline fluorescence. Then, the container was filled with water of different stimulation temperatures with the same average flow rate. Water-based stimulation was maintained for 60 s for each stimulation temperature. At the end of each trial, the viability and virus infection efficiency were confirmed by assessing calcium responses in DRG neurons triggered by hindpaw pinch.

Data analysis. The raw image stacks were imported into FIJI (NIH) for further analysis. The optical sections of sequential time points were realigned, and motion corrected using a cross-correlation-based image alignment plugin in FIJI to adjust for minor motion shifts during recording. The corrected four optical sections from sequential time points were processed with *z* projection to obtain the final whole DRG neuron image in time-lapse movies. The amplitudes of the calcium transient signal were calculated as $\Delta F/F$, where $\Delta F/F = (F_t - F_0)/F_0$. F_t was the maximum fluorescence intensity measured by calculating the average pixel values (peak intensity − background) of the chosen region of interest (ROI) for each frame recorded, and F_0 was the average fluorescence intensity of each ROI in the baseline period recorded 10–20 frames before temperature stimulation. Responding neurons were defined by the fluorescence intensity increase $\Delta F/F \geq 0.2$.

RNAscope in situ hybridization and immunohistochemistry

Mice were euthanized with CO_2 and perfused with PBS followed with 4% PFA (4 °C) in PBS. L3 to L5 DRGs were extracted and postfixed in 4% PFA for 2 h at 4 °C. DRGs were then incubated in 20% sucrose for dehydration. DRGs were sectioned into 14-µm slices using a Cryostat (Leica Microsystems) and mounted onto SuperFrost Plus microscope slides. The RNAscope system (Advanced Cell Diagnostics) was used according to the manufacturer's protocol. The mounting slices were pretreated with hydrogen peroxide and protease IV provided by the RNAscope Multiplex Fluorescent Reagent v2 assay kit (Advanced Cell Diagnostics). Samples were hybridized with a GluK2 messenger RNA probe (*GRIK2*-O_2-C1) customized with targeted sequences or *TRMP8*-C3/*TRPA1*-C2 probe for 2 h. Samples were further incubated with AMP1, AMP2 or AMP3 for 15–30 min, and HRP-C1, HRP-C2 or HRP-C3 for 15 min. Opal Dye 570 (1:1,500; cat. no. FP1488001KT) or

TSA Plus Cy5 (1:1,500; cat. no. NEL745E001KT) was added, incubated for 30 min and HRP blocked for 15 min. All the reagents were incubated in a 40 °C hybridization oven. To quantify positive neuron populations, neurons with more than three positive signals (observed as puncta) within the periphery of the neuron (determined by the phase contrast image) were considered as positive. Following RNAscope in situ hybridization, immunostaining was performed using the methods described previously[10]. Primary antibodies were used at the following concentrations: rabbit anti-NF200 antibody (1:500, cat. no. N4142, Millipore Sigma), rabbit anti-CGRP antibody (1:500, cat. no. PC205L, Millipore Sigma), IB4-Alexa Fluor 647 (1:500, cat. no. I32450, Thermo Fisher), Guinea pig anti-TRPV1 (VR1) antibody (1:500, cat. no. ACC-030-GP, Alomone Labs). Nuclear counterstaining was performed with DAPI solution provided by the RNAscope Multiplex Fluorescent Reagent v2 assay kit for 5 min. DRG sections were then mounted and imaged by fluorescence microscopy (Leica DMi8 and Olympus FV3000). Data were quantified with LAS X Life Science Microscope software (Leica Microsystems).

Single-cell RNA sequencing analysis

Raw single-cell RNA sequencing data in the form of .h5 files were obtained from a previously published article[15]. These files contained preprocessed gene expression matrices and relevant metadata. Data preprocessing was initiated by loading the .h5 files into R using the rhdf5 tool. The initial quality control steps were performed, including filtering out low-quality cells based on criteria such as gene count (fewer than 200 genes) and mitochondrial gene content (greater than 5%). Subsequent steps included normalization, scaling and dimensionality reduction using principal component analysis and Uniform Manifold Approximation and Projection (UMAP), as implemented in the Seurat pipeline. The preprocessed data were subjected to clustering analysis using Seurat's FindNeighbors and FindClusters functions, with a default clustering resolution parameter. Further data analysis and visualization were performed using R with the Seurat package and the ShineyCell package[47]. We mapped GluK2 mRNA (*GRIK2*) expression in known subsets of DRG neurons such as myelinated neurons (NF classes, $Ldhb^{High}$), *TRPM8*, *TRPA1* and *TRPV1* (ref. 15). To calculate the percentage of overlap between the *GRIK2*-expressing neurons and other sensory neuron markers, we used a single-cell RNA analysis tool, miCV[48]. We investigated the coexpression of *GRIK2* in the $Ldhb^{High}$ (normalized expression above 6), *TRPM8*, *TRPV1* and $TRPA1^{High}$ (normalized expression above 4) populations. Expression thresholds for *Ldhb* and *TRPA1* were defined to overcome the ambiguity caused by the noise created by cells showing low or very-low expression in false-positive cells.

Statistical analysis

Statistical methods, error bars (s.e.m.), *P* values and sample sizes (*n* number) are indicated in the figure legends. One-way analysis of variance (ANOVA) with Tukey's test, Student's *t*-tests and chi-squared tests were applied separately to analyze data, and are described in the figure legends. Both the one-way ANOVA and chi-squared tests used were two-sided. No data were excluded from statistical analysis. A *P* value less than 0.05 was considered statistically significant, $^{*}P < 0.05$, $^{**}P < 0.01$, $^{\#}P < 0.05$, $^{\#\#}P < 0.01$. All data were presented as mean ± s.e.m. and analyzed with GraphPad Prism 8.0 software (GraphPad). Mice were randomly allocated to different experimental groups. Data collection and analysis were performed blind to the conditions of the experiments in behavioral tests and in vitro calcium imaging. No statistical methods were used to predetermine sample sizes, but our sample sizes are similar to those reported in previous publications[17]. Data distribution was assumed to be normal, but this was not formally tested.

Reporting summary

Further information on research design is available in the Nature Portfolio Reporting Summary linked to this article.

Data availability

All the data generated or analyzed in this study are included in the figures, texts and Supplementary Information files. Additional data supporting the findings of this study are available upon reasonable request.

References

42. Marshall, J. J., Xu, J. & Contractor, A. Kainate receptors inhibit glutamate release via mobilization of endocannabinoids in striatal direct pathway spiny projection neurons. *J. Neurosci.* **38**, 3901–3910 (2018).
43. Kim, A. Y. et al. Pirt, a phosphoinositide-binding protein, functions as a regulatory subunit of TRPV1. *Cell* **133**, 475–485 (2008).
44. Pan, H. et al. Identification of a spinal circuit for mechanical and persistent spontaneous itch. *Neuron* **103**, 1135–1149 e1136 (2019).
45. Chaplan, S. R., Bach, F. W., Pogrel, J. W., Chung, J. M. & Yaksh, T. L. Quantitative assessment of tactile allodynia in the rat paw. *J. Neurosci. Methods* **53**, 55–63 (1994).
46. Ran, C., Hoon, M. A. & Chen, X. The coding of cutaneous temperature in the spinal cord. *Nat. Neurosci.* **19**, 1201–1209 (2016).
47. Ouyang, J. F., Kamaraj, U. S., Cao, E. Y. & Rackham, O. J. L. ShinyCell: simple and sharable visualization of single-cell gene expression data. *Bioinformatics* **37**, 3374–3376 (2021).
48. Michki, N. S. et al. The molecular landscape of neural differentiation in the developing *Drosophila* brain revealed by targeted scRNA-seq and multi-informatic analysis. *Cell Rep.* **35**, 109039 (2021).

Acknowledgements

We thank A. Contractor for providing GluK2-floxed mice; S. Tomita for providing GluK2 KO mice; and J. Feng, Z. Xie, H. Hu and M. Zhang for technical assistance and discussion. This work was supported by the NINDS (to X.Z.S.X. and B.D.) and NIGMS (to X.Z.S.X.).

Author contributions

W.C. performed most behavioral tests, conducted in vitro DRG imaging experiments and analyzed the data. W.Z. performed water droplet behavior tests, whole-cell recordings and RNAscope in situ hybridization, and analyzed the data. Q.Z. and X.D. performed in vivo DRG imaging experiments, and analyzed the data with W.C. and W.Z. C.C.H. assisted W.C. and W.Z. with behavioral tests. T.P. assisted W.C. with in vitro DRG imaging experiments. M.F. analyzed RNA-seq data and assisted W.Z. with RNAscope in situ hybridization. B.D. and X.Z.S.X. supervised the project. W.C., W.Z., B.D. and X.Z.S.X. wrote the paper with assistance from all other authors.

Competing interests

The authors declare no competing interests.

Additional information

Extended data is available for this paper at https://doi.org/10.1038/s41593-024-01585-8.

Supplementary information The online version contains supplementary material available at https://doi.org/10.1038/s41593-024-01585-8.

Correspondence and requests for materials should be addressed to Bo Duan or X.Z. Shawn Xu.

Peer review information *Nature Neuroscience* thanks Diana Bautista, Ryan Pak, Raul Ramos, Nick Villarino and the other, anonymous, reviewer(s) for their contribution to the peer review of this work.

https://doi.org/10.1038/s41593-024-01585-8

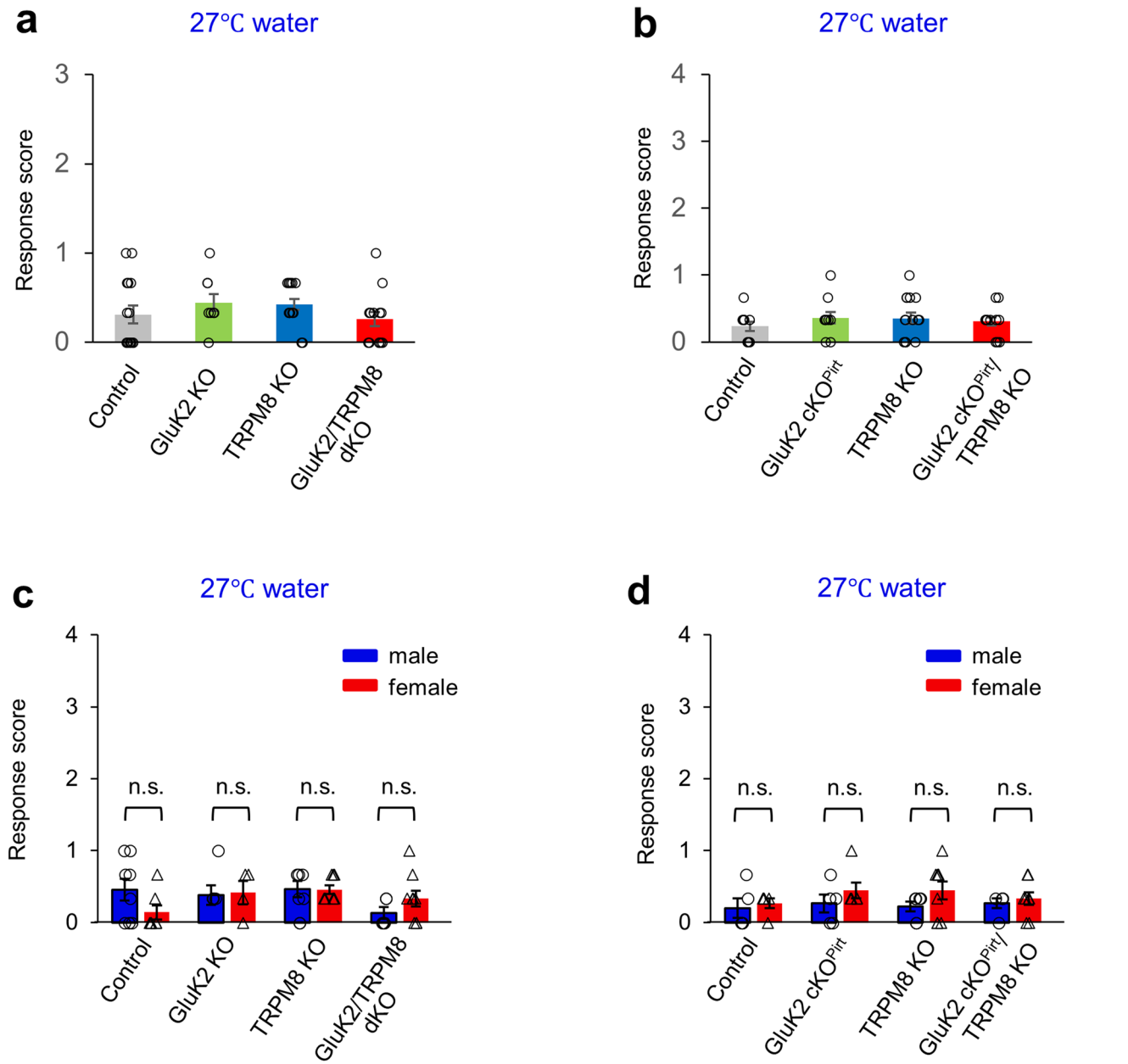

Extended Data Fig. 1 | Mice show no response to water droplet stimuli near the temperature of their paw's skin surface, and there is no observed difference between males and females. (a, b) Water droplet stimuli at 27 °C are applied to mouse hindpaw using a syringe. Each mouse was tested three times, and the resulting score is calculated as the average of these tests. Error bars: SEM. $P > 0.05$ (not statistically significant; one-way ANOVA with Tukey test). Sample sizes in (a): control n = 15, TRPM8 KO n = 15, GluK2 KO n = 9, GluK2/TRPM8 dKO n = 14 (mice). Sample sizes in (b): control n = 10, TRPM8 KO n = 15, GluK2 cKO^{Pirt} n = 11, GluK2 cKO^{Pirt}/TRPM8 dKO n = 13 (mice). **(c, d)** No notable difference was observed between males and females. n.s. not statistically significant ($P > 0.05$; one-way ANOVA with Tukey test). Data in (a) and (b) are grouped separately as male and female cohorts for each genotype and analyzed separately. Sample sizes in (c): control male n = 8, control female n = 7, TRPM8 KO male n = 7, TRPM8 KO female n = 8, GluK2 KO male n = 5, GluK2 KO female n = 4, GluK2/TRPM8 dKO male n = 5, GluK2/TRPM8 dKO female n = 9 (mice). Sample sizes in (d): control male n = 5, control female n = 5, TRPM8 KO male n = 6, TRPM8 KO female n = 9, GluK2 cKO^{Pirt} male n = 5, GluK2 cKO^{Pirt} female n = 6, GluK2 cKO^{Pirt}/TRPM8 KO male n = 5, GluK2 cKO^{Pirt}/TRPM8 KO female n = 8 (mice). Error bars: SEM. Data are presented as mean ± SEM.

https://doi.org/10.1038/s41593-024-01585-8

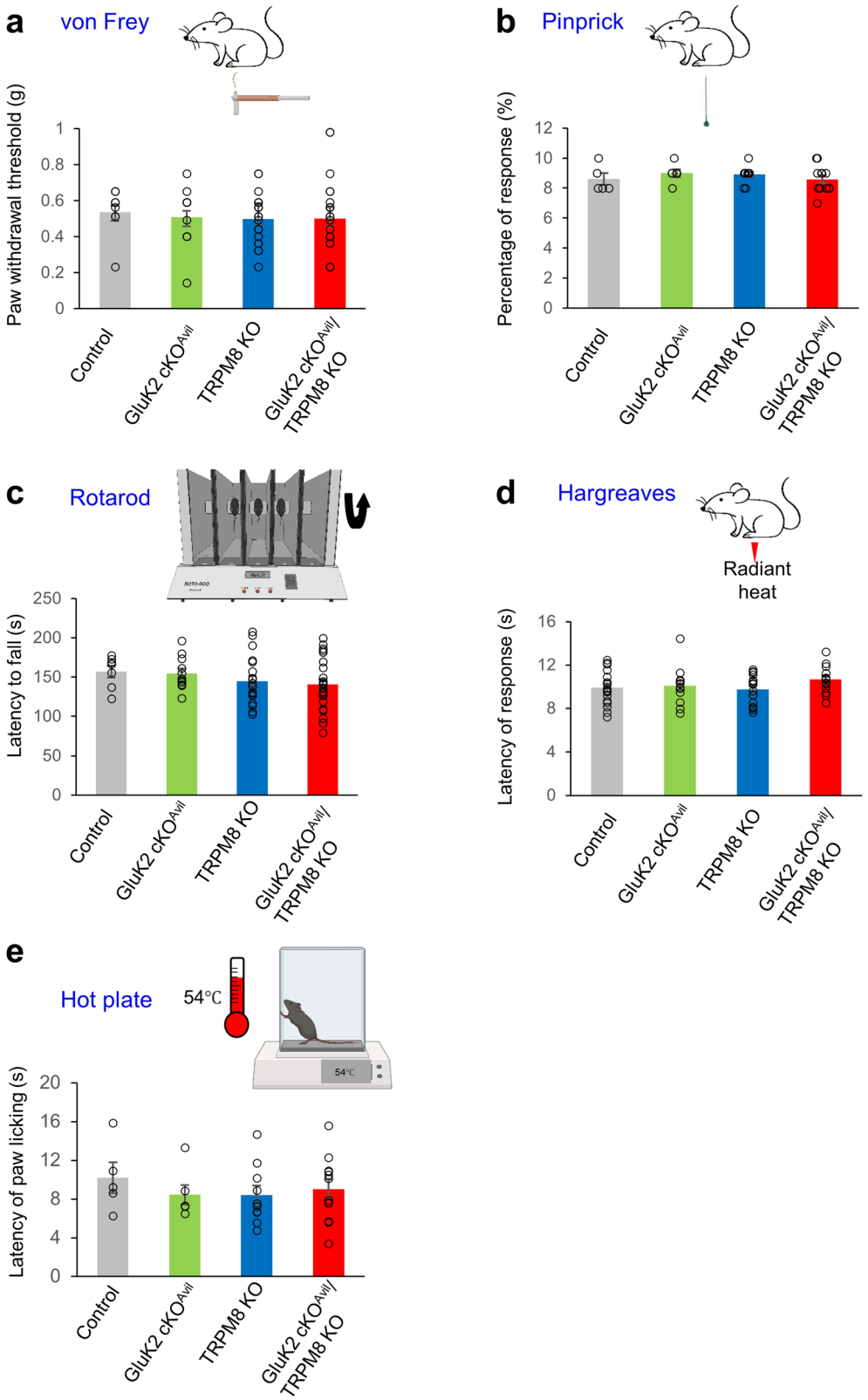

Extended Data Fig. 2 | GluK2 cKO^{Avil} mice respond normally to mechanical and heat stimuli and behave normally in the rotarod test. **(a)** The von Frey test (control: n = 8; GluK2 cKO^{Avil}: n = 11; TRPM8 KO: n = 20; GluK2 cKO^{Avil}/TRPM8 KO: n = 24). **(b)** The pinprick test (control: n = 5; GluK2 cKO^{Avil}: n = 6; TRPM8 KO: n = 10; GluK2 cKO^{Avil}/TRPM8 KO: n = 12). **(c)** The rotarod test (control: n = 7; GluK2 cKO^{Avil}: n = 11; TRPM8 KO: n = 19; GluK2 cKO^{Avil}/TRPM8 KO: n = 24). **(d)** The Hargreaves test (control: n = 18; GluK2 cKO^{Avil}: n = 14; TRPM8 KO: n = 18; GluK2 cKO^{Avil}/TRPM8 KO: n = 14). **(e)** The hot plate test (control: n = 5; GluK2 cKO^{Avil}: n = 6; TRPM8 KO: n = 10; GluK2 cKO^{Avil}/TRPM8 KO: n = 12). Error bars: SEM. P values: all >0.05 (not statistically significant; one-way ANOVA with Tukey test). Data are presented as mean ± SEM.

https://doi.org/10.1038/s41593-024-01585-8

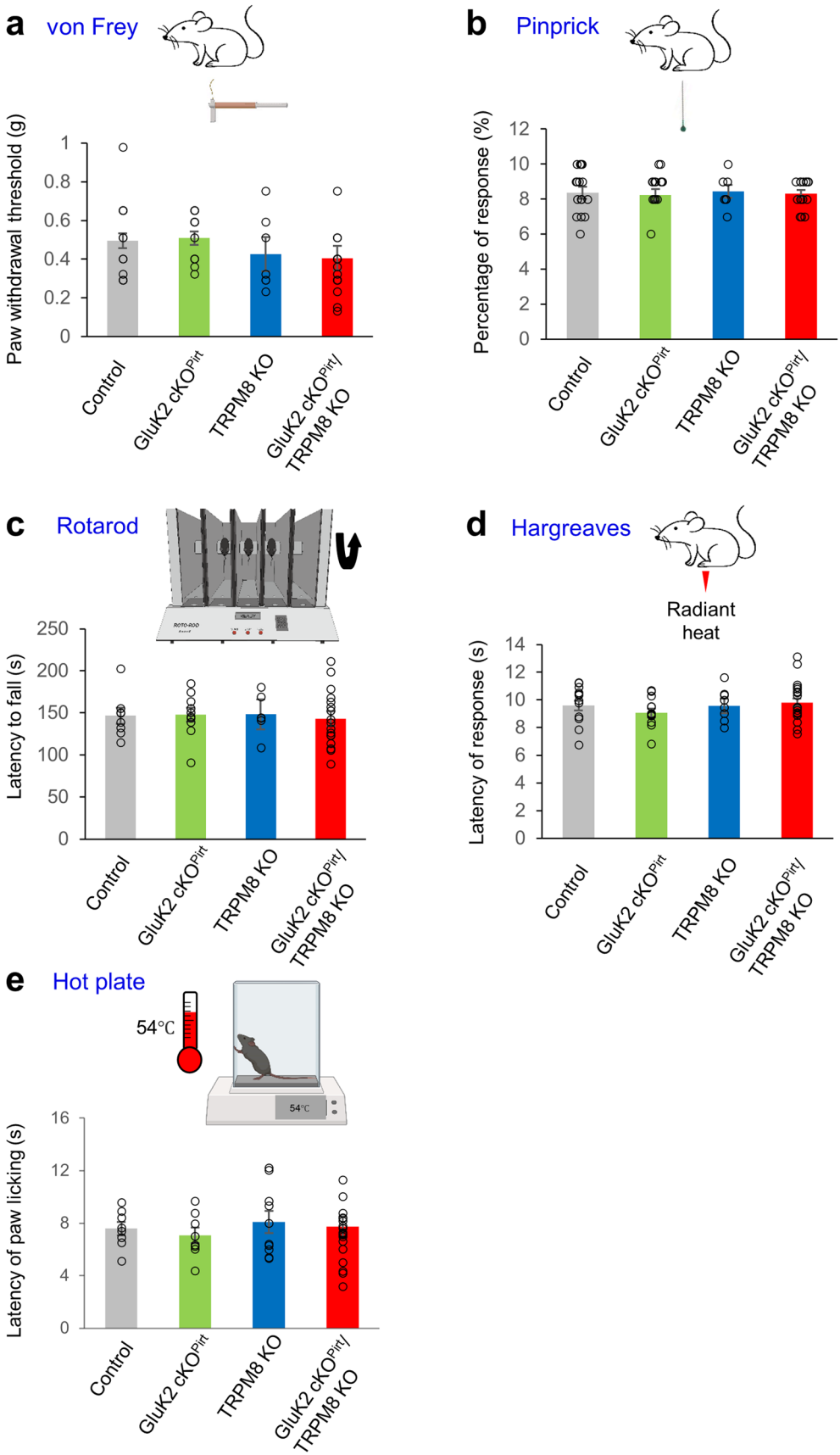

Extended Data Fig. 3 | See next page for caption.

https://doi.org/10.1038/s41593-024-01585-8

Extended Data Fig. 3 | GluK2 cKO^{Pirt} mice respond normally to mechanical and heat stimuli and behave normally in the rotarod test. (a) The von Frey test (control: n = 12; GluK2 cKO^{Pirt}: n = 12; TRPM8 KO: n = 7; GluK2 cKO^{Pirt}/TRPM8 KO: n = 19). **(b)** The pinprick test (control: n = 14; GluK2 cKO^{Pirt}: n = 9; TRPM8 KO: n = 7; GluK2 cKO^{Pirt}/TRPM8 KO: n = 16). **(c)** The rotarod test (control: n = 8; GluK2 cKO^{Pirt}: n = 10; TRPM8 KO: n = 6; GluK2 cKO^{Pirt}/TRPM8 KO: n = 17). **(d)** The Hargreaves test (control: n = 12; GluK2 cKO^{Pirt}: n = 12; TRPM8 KO: n = 8; GluK2 cKO^{Pirt}/TRPM8 KO: n = 20). **(e)** The hot plate test (control: n = 8; GluK2 cKO^{Pirt}: n = 8; TRPM8 KO: n = 10; GluK2 cKO^{Pirt}/TRPM8 KO: n = 20). Error bars: SEM. P-values: all >0.05 (not statistically significant; one-way ANOVA with Tukey test). Data are presented as mean ± SEM.

https://doi.org/10.1038/s41593-024-01585-8

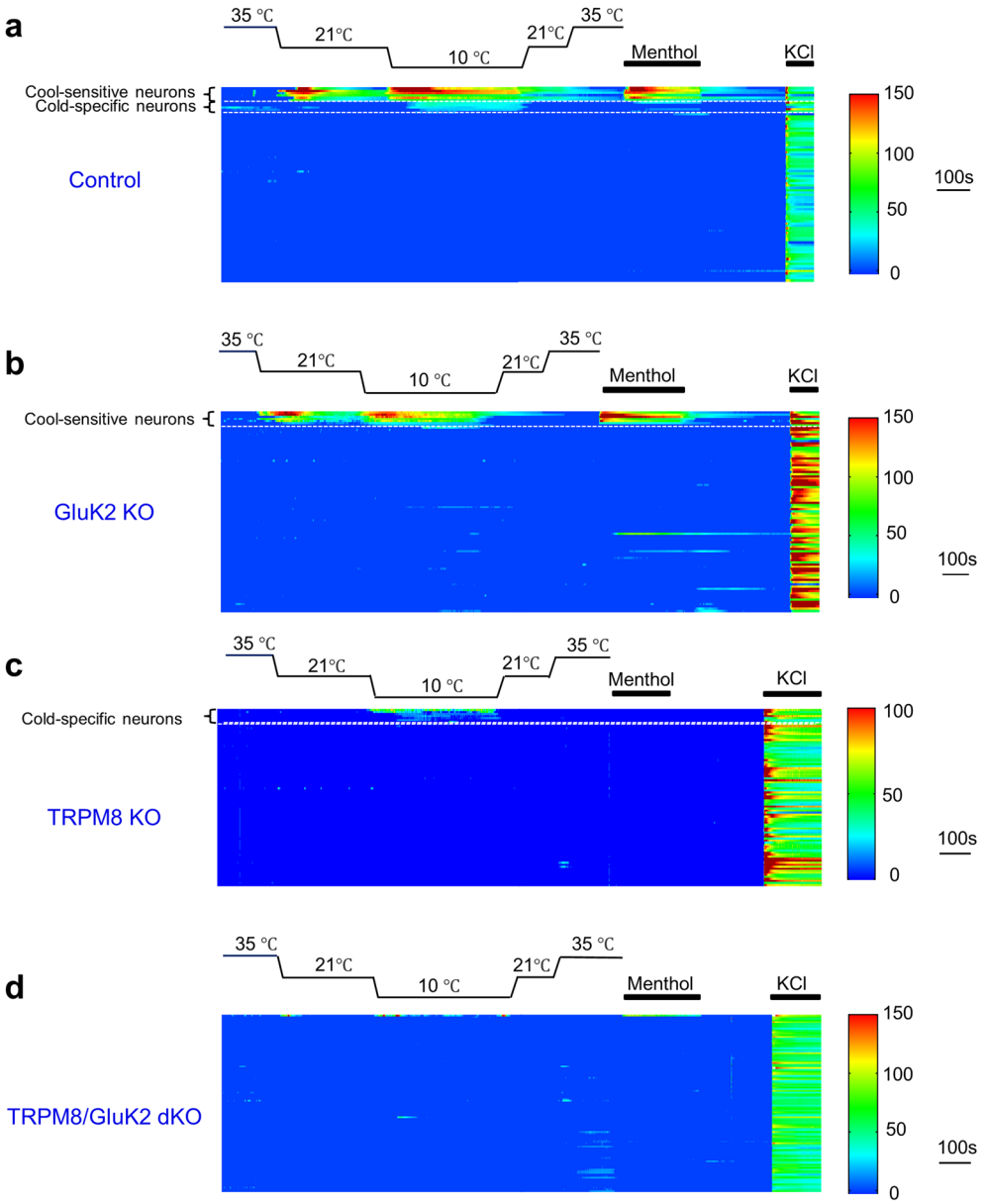

Extended Data Fig. 4 | Heat map of in vitro calcium imaging data (related to Fig. 4). Dissociated DRG neurons were recorded by calcium imaging as described in Fig. 4. The data from all recorded DRG neurons from one representative mouse was presented as a heat map for each genotype. **(a)** Control. **(b)** GluK2 KO. **(c)** TRPM8 KO. **(d)** GluK2/TRPM8 dKO.

https://doi.org/10.1038/s41593-024-01585-8

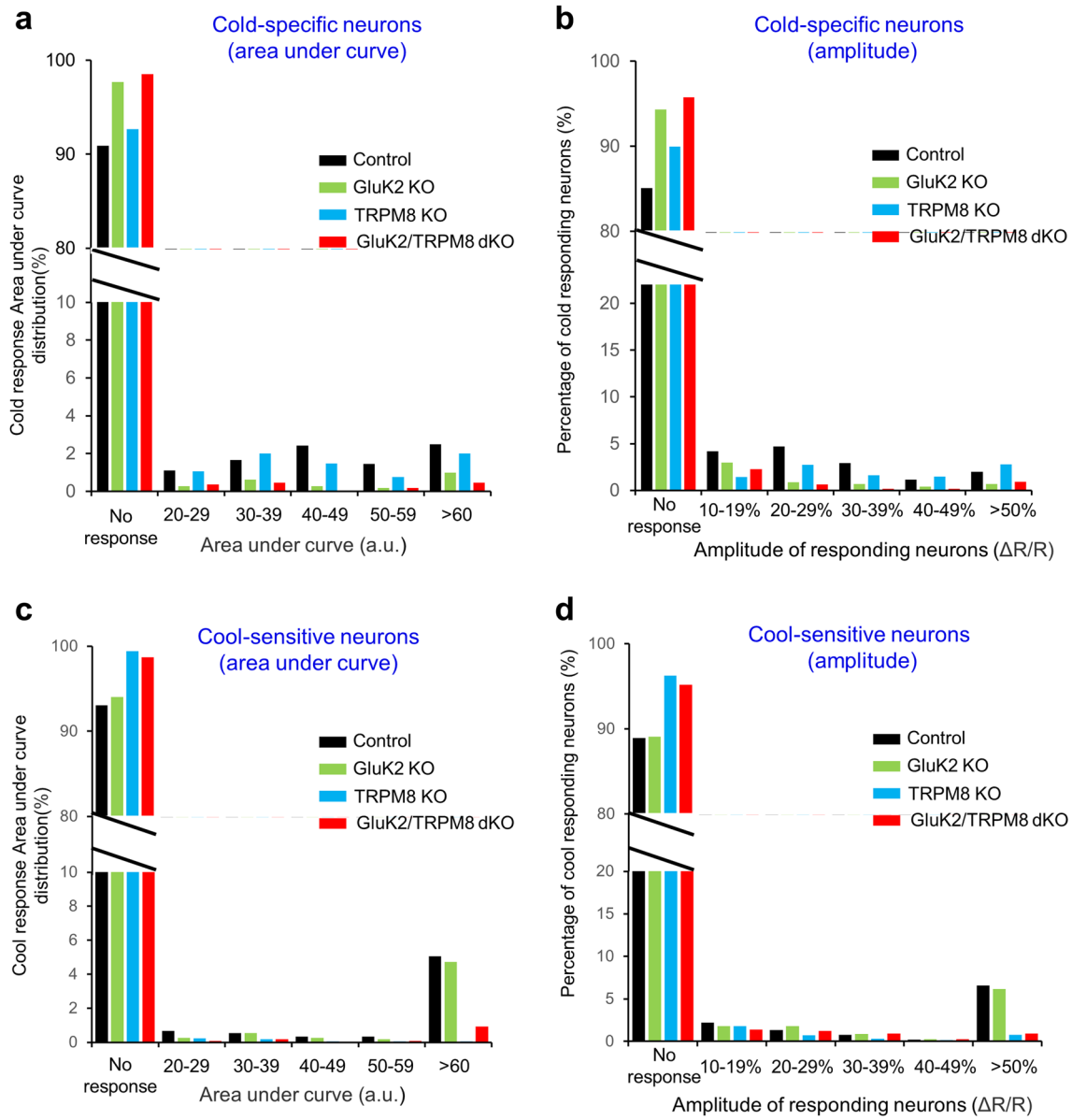

Extended Data Fig. 5 | Quantification of area under curve and amplitude of in vitro calcium imaging data (related to Fig. 4). (a) Area under curve distribution of cold-specific DRG neurons. **(b)** Amplitude distribution of cold-specific DRG neurons. **(c)** Area under curve distribution of cool-sensitive DRG neurons. **(d)** Amplitude distribution of cool-sensitive DRG neurons. Neurons with an amplitude lower than 10% (ΔR/R) (<20 a.u. for area under curve) were considered no response as it was difficult to resolve signals from noises in these cases. Neurons with an amplitude at least 20% ((ΔR/R) were included for analysis in Fig. 4 (see Methods). Control: 2361 neurons; GluK2 KO: 1119 neurons; TRPM8 KO: 1681 neurons; GluK2/TRPM8 dKO: 1063 neurons.

https://doi.org/10.1038/s41593-024-01585-8

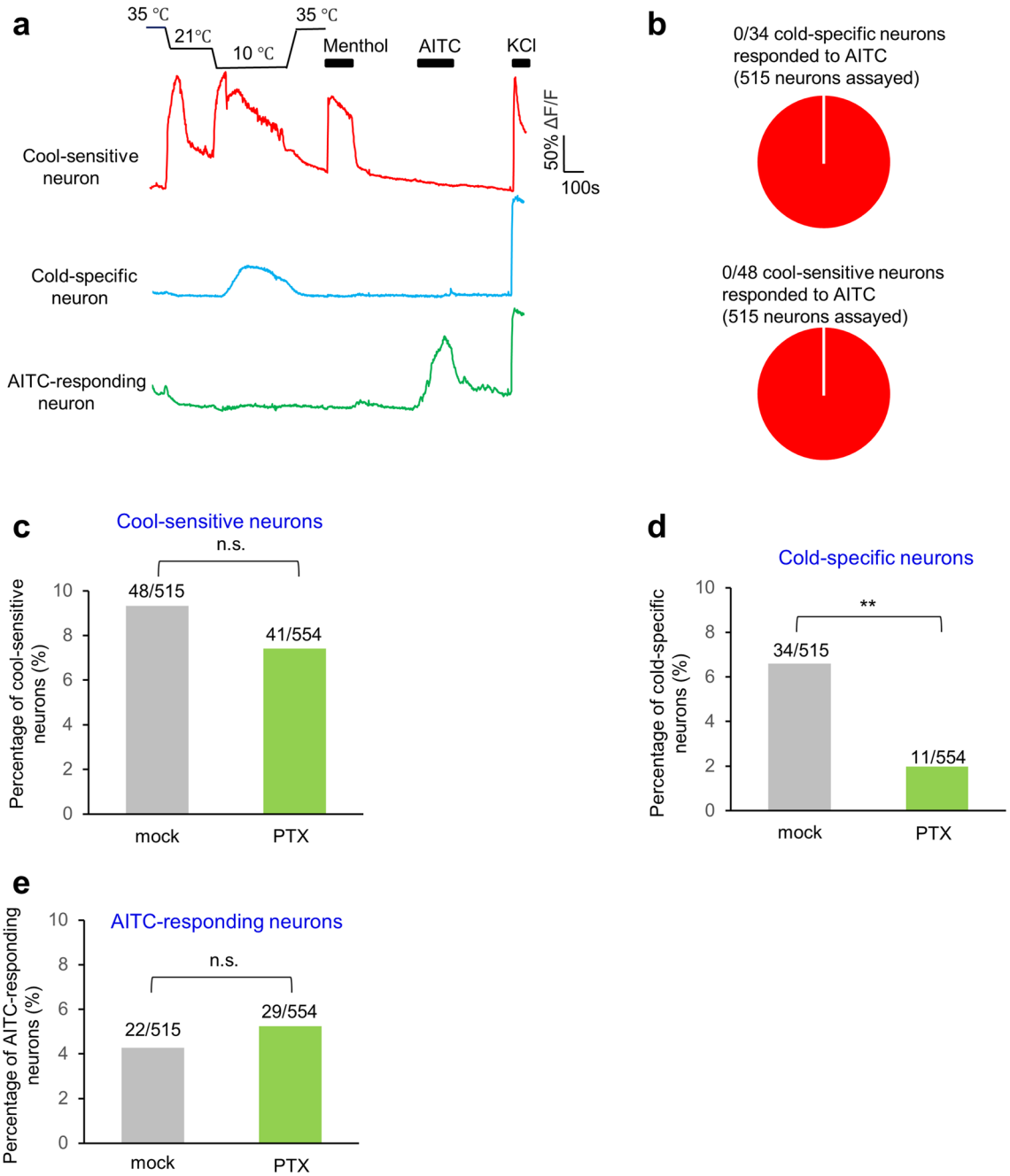

Extended Data Fig. 6 | Quantification of AITC-responding DRG neurons and the effect of PTX (pertussis toxin) on cool-sensitive and cold-specific DRG neurons. Calcium imaging was performed on dissociated DRG neurons using the protocol described in Fig. 4. AITC (100 μM) and menthol (100 μM) were applied acutely to DRG neurons during calcium imaging. PTX (100 ng/ml) was pre-incubated with DRG neurons for 6 hours prior to calcium imaging. KCl (50 mM) was added at the end of the experiment to validate the health of DRG neurons. **(a)** Sample traces of cool-sensitive, cold-specific and AITC-responding DRG neurons. **(b)** Quantification of cool-sensitive and cold-specific DRG neurons that responded to AITC. **(c)** The percentage cool-sensitive DRG neurons is not significantly affected by PTX. **(d)** The percentage cold-specific DRG neurons is greatly reduced by PTX. **(e)** The percentage AITC-responding DRG neurons is not significantly affected by PTX. The numbers of responding and non-responding neurons are indicated in each panel (from 7 mice). n.s.: no significant difference ($p > 0.05$; Chi-square test). **$p = 0.000173$, PTX vs mock group (Chi-square test).

https://doi.org/10.1038/s41593-024-01585-8

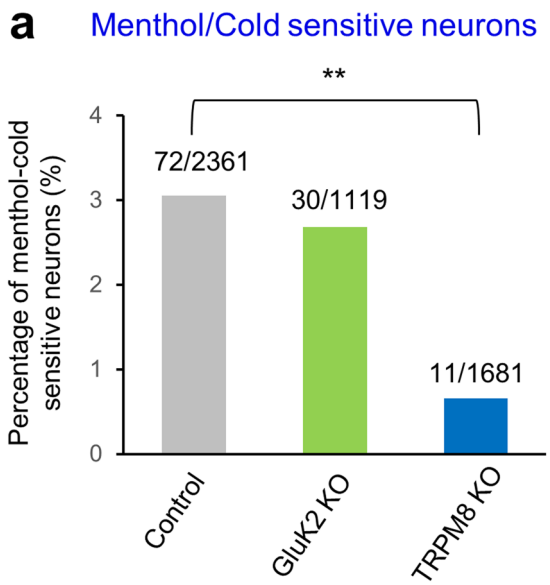

Extended Data Fig. 7 | A small population of menthol/cold-sensitive DRG neurons is dependent on TRPM8 but not GluK2. (a) In experiments described in Fig. 4,we also identified a small population of DRG neurons that were insensitive to cool temperatures but sensitive to menthol and cold temperatures. The number of responding neurons and total neurons assayed is indicated for each genotype. Wild-type littermate mice are used as control. Error bars: SEM. Control: n = 31 (mice); GluK2 KO: n = 15 (mice); TRPM8 KO: n = 19 (mice): GluK2/TRPM8 dKO: n = 10 (mice). **p = 1.21E-07 TRPM8 KO vs Control group (Chi-square test).

https://doi.org/10.1038/s41593-024-01585-8

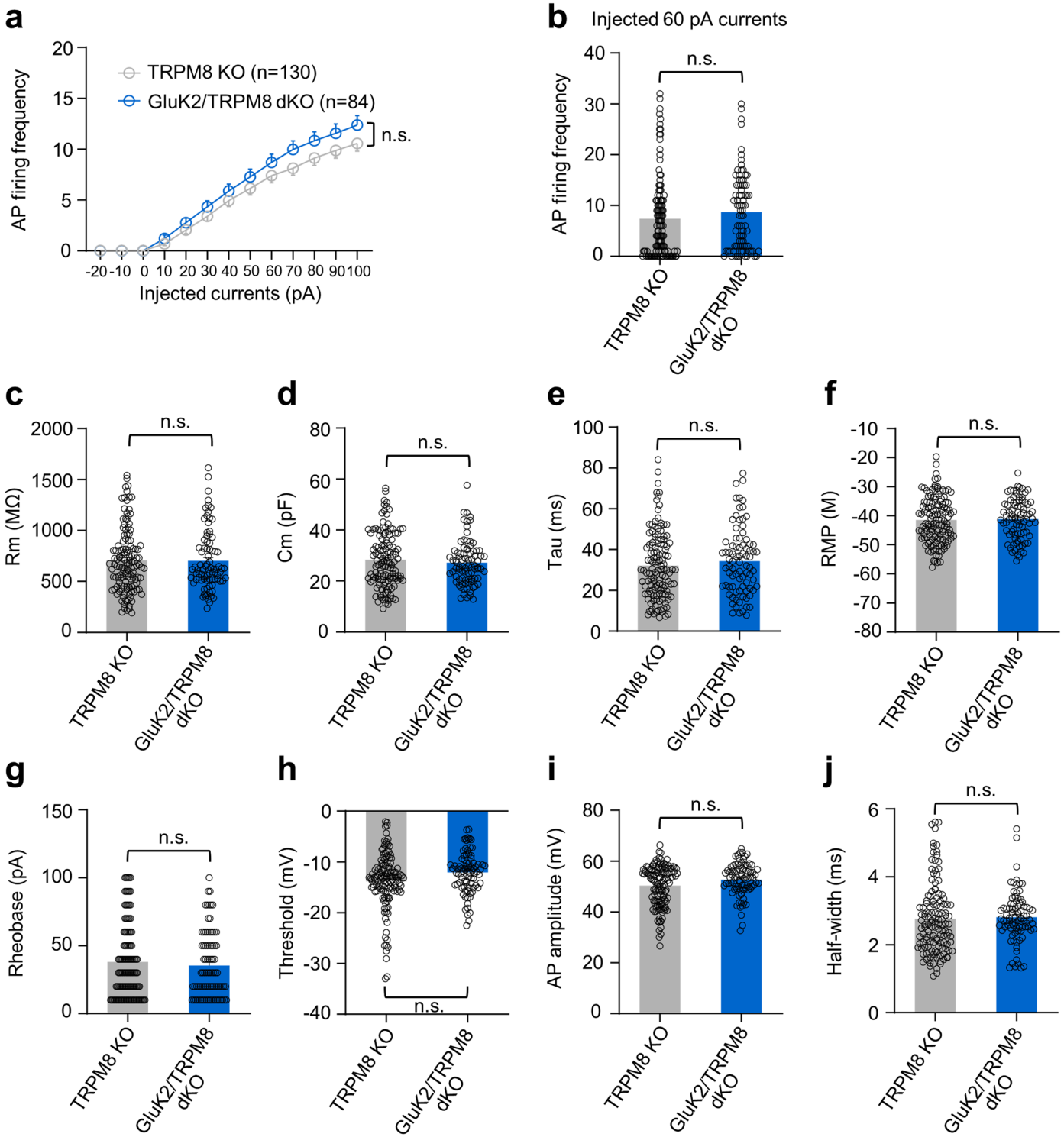

Extended Data Fig. 8 | No significant differences are observed in the intrinsic properties and excitability of dissociated DRG neurons from TRPM8 KO and GluK2/TRPM8 dKO mice (related to Fig. 5). **(a)** Whole-cell patch recording of action potential (AP) firing frequency induced by injected current steps. **(b)** AP firing frequency induced by 60 pA injected currents. **(c-f)** Quantification of the membrane resistance **(c)**, membrane capacitance **(d)**, time constant **(e)**, and resting membrane potential **(f)** of recorded neurons. **(g)** Quantification of the first step current that induced AP (Rheobase) in recorded neurons. **(h-j)** Quantification of the threshold **(h)**, amplitude **(i)** and half-width **(j)** of the first induced AP. Error bars: SEM. n.s.: no significant difference ($P > 0.05$; two-tailed Student's *t*-test). Sample size: n = 130 neurons (TRPM8 KO; 11 mice); n = 84 neurons (GluK2/TRPM8 dKO; 6 mice). Data are presented as mean ± SEM.

https://doi.org/10.1038/s41593-024-01585-8

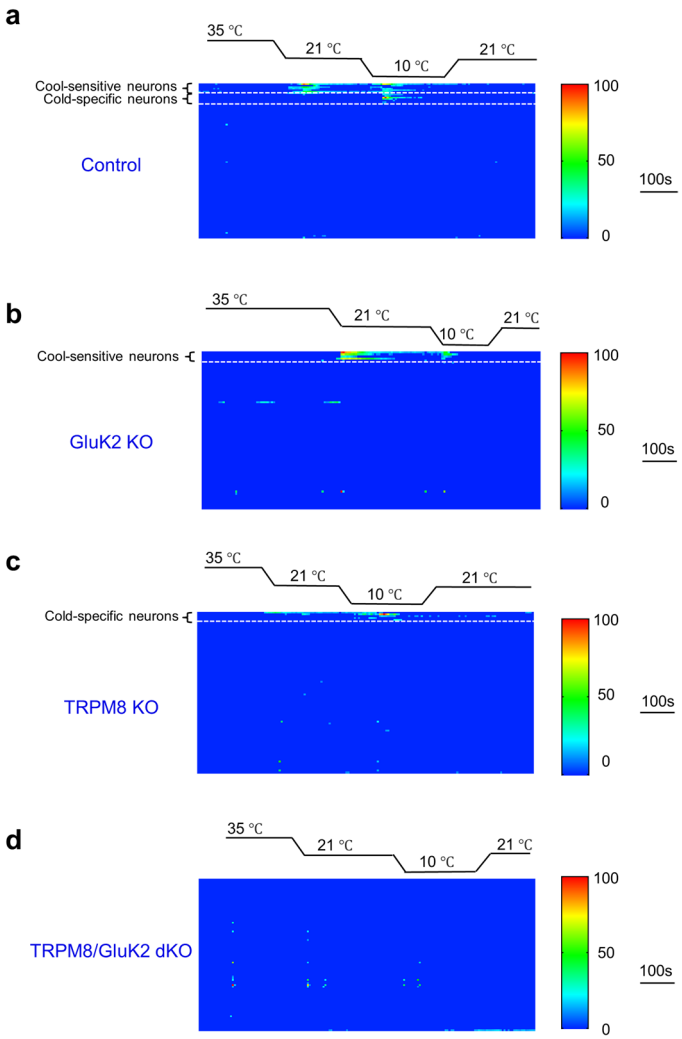

Extended Data Fig. 9 | Heat map of in vivo calcium imaging data (related to Fig. 6). In vivo calcium imaging of DRG neurons was performed as described in Fig. 6. The data from all imaged DRG neurons from one representative mouse was presented as a heat map for each genotype. **(a)** Control: wild-type littermate. **(b)** GluK2 KO. **(c)** TRPM8 KO. **(d)** GluK2/TRPM8 dKO.

https://doi.org/10.1038/s41593-024-01585-8

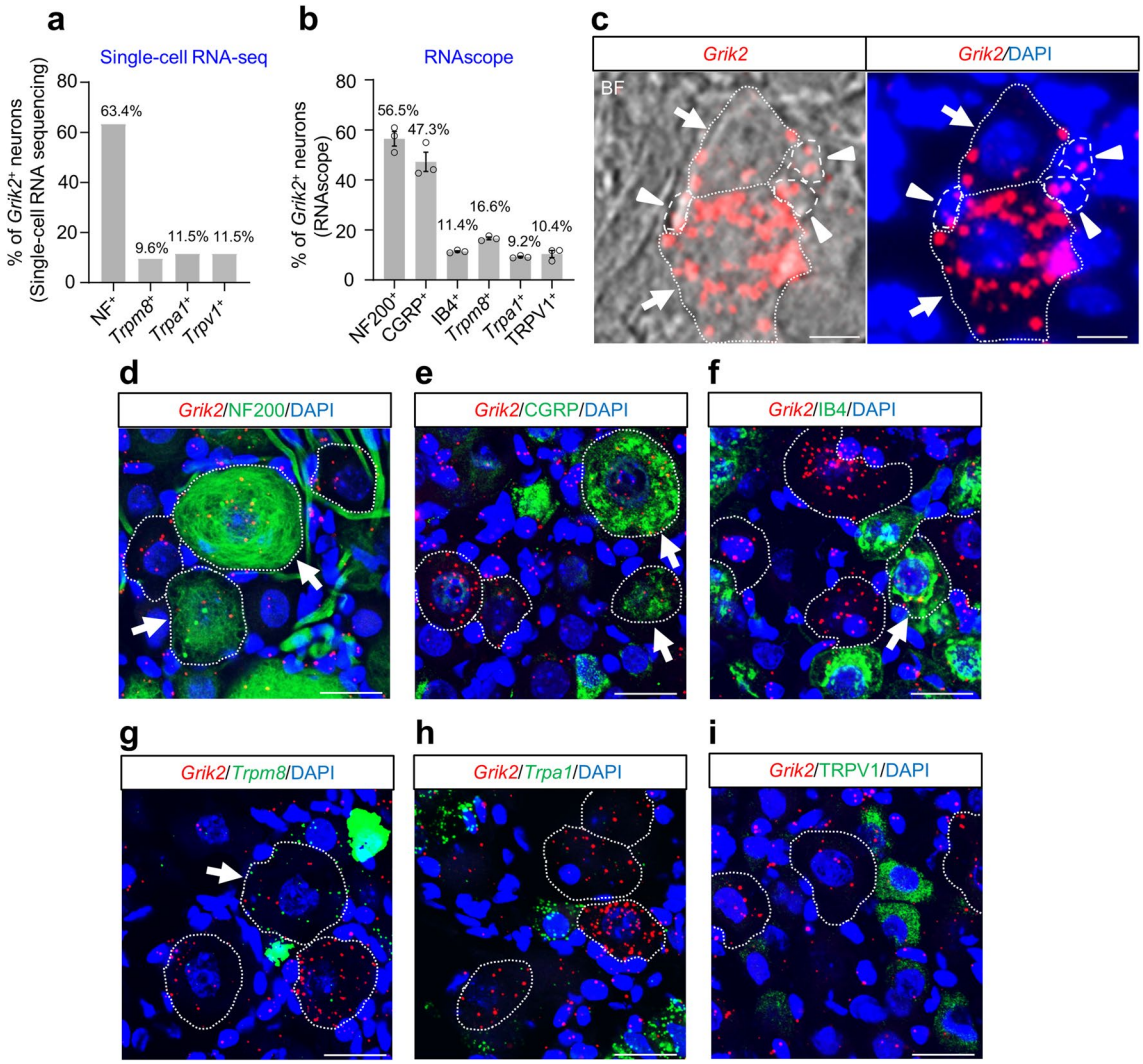

Extended Data Fig. 10 | GluK2 mRNA (*Grik2*) expression pattern in the DRG determined by single-cell RNA-seq and RNAscope *in situ* hybridization. **(a)** Quantification of single-cell RNA-seq data from published work (ref. 15) shows that GluK2 mRNA (*Grik2*) positive neurons partially co-localize with myelinated neuron populations (NF), but exhibit little co-localization with TRPM8 mRNA (*Trpm8*), TRPA1 mRNA (*Trpa1*) and TRPV1 mRNA (*Trpv1*) in mouse DRGs. The percentages of colocalization with each marker are indicated. The CGRP mRNA (*Calca*) positive DRG neuron population is not analyzed due to inconsistency. **(b-i)** Quantification of GluK2 mRNA (*Grik2*) positive neuron population colocalization with various markers in mouse DRGs, including NF200, CGRP, IB4, TRPM8 mRNA (*Trpm8*), TRPA1 mRNA (*Trpa1*) and TRPV1. Neurons with more than three positive signals (observed as puncta) within the periphery of the neurons (determined by the phase contrast image) were considered as positive. **(b)** Bar graph summarizing the percentages of colocalization of GluK2 mRNA (*Grik2*) positive neuron with each marker. n = 3 (mice). Error bars: SEM. Data are presented as mean ± SEM. **(c)** GluK2 mRNA (*Grik2*) is expressed in neurons as well as some glial cells. About 26% of DRG neurons express GluK2 mRNA (data was quantified with 3 mice). GluK2 mRNA-positive neurons (indicated by white dotted lines) and glial cells (represented by white long broken lines) are distinguished using bright field (BF, left) and fluorescent images (right) with DAPI staining, based on their morphology and nucleus characteristics. White arrows indicate GluK2 mRNA-positive neurons and white arrow heads indicate GluK2 mRNA-positive glial cells. Scale bar: 10 μm. **(d-i)** Representative RNAscope images show colocalization of GluK2 mRNA-positive neurons with NF200 **(d)**, CGRP **(e)**, IB4 **(f)**, TRPM8 mRNA **(g)**, TRPA1 mRNA **(h)**, and TRPV1 **(i)** in DRG neurons. White dotted lines label GluK2 mRNA-positive neurons, while white arrows indicate overlayed neurons. Scale bar: 20 μm.

nature portfolio

Corresponding author(s): Bo Duan & X.Z. Shawn Xu

Last updated by author(s): Dec 20, 2023

Reporting Summary

Nature Portfolio wishes to improve the reproducibility of the work that we publish. This form provides structure for consistency and transparency in reporting. For further information on Nature Portfolio policies, see our Editorial Policies and the Editorial Policy Checklist.

Statistics

For all statistical analyses, confirm that the following items are present in the figure legend, table legend, main text, or Methods section.

n/a	Confirmed
☐	☒ The exact sample size (*n*) for each experimental group/condition, given as a discrete number and unit of measurement
☐	☒ A statement on whether measurements were taken from distinct samples or whether the same sample was measured repeatedly
☐	☒ The statistical test(s) used AND whether they are one- or two-sided *Only common tests should be described solely by name; describe more complex techniques in the Methods section.*
☐	☒ A description of all covariates tested
☐	☒ A description of any assumptions or corrections, such as tests of normality and adjustment for multiple comparisons
☐	☒ A full description of the statistical parameters including central tendency (e.g. means) or other basic estimates (e.g. regression coefficient) AND variation (e.g. standard deviation) or associated estimates of uncertainty (e.g. confidence intervals)
☐	☒ For null hypothesis testing, the test statistic (e.g. *F*, *t*, *r*) with confidence intervals, effect sizes, degrees of freedom and *P* value noted *Give P values as exact values whenever suitable.*
☒	☐ For Bayesian analysis, information on the choice of priors and Markov chain Monte Carlo settings
☒	☐ For hierarchical and complex designs, identification of the appropriate level for tests and full reporting of outcomes
☒	☐ Estimates of effect sizes (e.g. Cohen's *d*, Pearson's *r*), indicating how they were calculated

Our web collection on statistics for biologists contains articles on many of the points above.

Software and code

Policy information about availability of computer code

Data collection	In vitro calcium imaging was performed with MetaFluor for Olympus(Version 7.8.2.2.0, Molecular Devices). In vivo calcium imaging was performed with Leica Application Suite X(Version 1.1.0.12420, Leica Microsystems). Two-temperature choice test was performed with BioT2CT(Version 2.2.6 Bioseb).
Data analysis	The in vitro calcium imaging results were analyzed using MetaFluor software from Olympus (Version 7.8.2.2.0, Molecular Devices). The results of the two-temperature choice test were analyzed with BioT2CT (Version 2.2.6 Bioseb). Data analysis for in vivo calcium imaging was performed using ImageJ (version 1.8.0). Microsoft Excel was utilized to process the data points from both the calcium imaging and behavioral tests.

For manuscripts utilizing custom algorithms or software that are central to the research but not yet described in published literature, software must be made available to editors and reviewers. We strongly encourage code deposition in a community repository (e.g. GitHub). See the Nature Portfolio guidelines for submitting code & software for further information.

Data

Policy information about availability of data

All manuscripts must include a data availability statement. This statement should provide the following information, where applicable:

- Accession codes, unique identifiers, or web links for publicly available datasets
- A description of any restrictions on data availability
- For clinical datasets or third party data, please ensure that the statement adheres to our policy

All the data generated or analyzed in this study are included in the figures, texts, and supplementary information files. Additional data supporting the findings of this study are available upon reasonable request.

Human research participants

Policy information about studies involving human research participants and Sex and Gender in Research.

Reporting on sex and gender	N/A
Population characteristics	N/A
Recruitment	N/A
Ethics oversight	N/A

Note that full information on the approval of the study protocol must also be provided in the manuscript.

Field-specific reporting

Please select the one below that is the best fit for your research. If you are not sure, read the appropriate sections before making your selection.

☒ Life sciences ☐ Behavioural & social sciences ☐ Ecological, evolutionary & environmental sciences

For a reference copy of the document with all sections, see nature.com/documents/nr-reporting-summary-flat.pdf

Life sciences study design

All studies must disclose on these points even when the disclosure is negative.

Sample size	Samples sizes are described in figure legends. No statistical methods were used to pre-determine sample sizes, but our sample sizes are similar to those reported in previous publications (ref 17)
Data exclusions	No data points were excluded from our analyses.
Replication	All experiments were replicated in five or more mice from at least three litters.
Randomization	Experimental and littermate control mice were maintained under the same conditions and allocated to treatments/groups randomly (for example, in two temperature plates test, control temperature and testing temperature distribute randomly).
Blinding	Mice were randomly allocated to different experimental groups. Data collection and analysis were performed blind to the conditions of the experiments in behavioral tests and in vitro calcium imaging.

Reporting for specific materials, systems and methods

We require information from authors about some types of materials, experimental systems and methods used in many studies. Here, indicate whether each material, system or method listed is relevant to your study. If you are not sure if a list item applies to your research, read the appropriate section before selecting a response.

Materials & experimental systems

n/a	Involved in the study
☐	☒ Antibodies
☒	☐ Eukaryotic cell lines
☒	☐ Palaeontology and archaeology
☐	☒ Animals and other organisms
☒	☐ Clinical data
☒	☐ Dual use research of concern

Methods

n/a	Involved in the study
☒	☐ ChIP-seq
☒	☐ Flow cytometry
☒	☐ MRI-based neuroimaging

Antibodies

Antibodies used	Rabbit anti-NF200 antibody (1:500, CAT# N4142, Millipore Sigma), rabbit anti-CGRP antibody (1:500, CAT# PC205L, Millipore Sigma), IB4-Alexa Fluor 647 (1:500, CAT# I32450, Thermo Fisher), Guinea pig anti-TRPV1 (VR1) antibody (1:500, CAT# ACC-030-GP, Alomone labs).
Validation	Each antibody has been widely used and reported. Relevant information is available on the vendor's website.

Animals and other research organisms

Policy information about studies involving animals; ARRIVE guidelines recommended for reporting animal research, and Sex and Gender in Research

Laboratory animals	Advillin-Cre (Jackson laboratory, # 032536), TRPM8 KO (Jackson laboratory, # 008198), Pirt-Cre mice were generated by Xinzhong Dong's lab at the John Hopkins University, GluK2 KO mice were kindly provided by Susumu Tomita's laboratory at Yale University, GluK2 floxed mice were kindly provided by Anis Contractor's lab at Northwestern University.
Wild animals	None
Reporting on sex	All experiments involved the use of both male and female mice, with the exception of Advillin-Cre mice. Only male mice were used in this case due to the germ-line leaky activity exhibited by female Advillin-Cre mice.
Field-collected samples	No field collected samples were used in this study.
Ethics oversight	All animal experiments were carried out according to the protocols (PRO00011268, PRO00011049, MO22M274) approved by the University of Michigan Institutional Animal Care and Use Committee and John Hopkins University Institutional Animal Care and Use Committee as consistent with the National Institutes of Health (NIH) Guidelines for the Care and Use of Laboratory Animals.

Note that full information on the approval of the study protocol must also be provided in the manuscript.